A SEARCH FOR FRACTIONALLY CHARGED PARTICLES

Richard Gerard Milner

In partial fulfillment of the Requirements
for the Degree of
Doctor of Philosophy

California Institute of Technology
Pasadena, California
1985
(Submitted Dec 10, 1984)

Acknowledgements

It is my pleasure to acknowledge the assistance, guidance, and direction of Dr. Robert D. McKeown. His arrival at Kellogg created an atmosphere in which an ambitious project as this could not only be considered, but also could be carried to fruition in a successful manner. I would also like to sincerely thank Dr. Barbara H. Cooper, who was instrumental in initiating this project. She worked for two years on this experiment, but unfortunately was unable to be here when the results were taken. I would like to express my admiration of Wil Schick and the Kellogg machine shop for the manner in which the many pieces for this experiment were expertly machined. We quickly learned that the tolerances and quality of work coming out of the Kellogg shop far surpassed those of commercially available equipment. I would like to acknowledge the contribution of Dr. Kai H. Chang, who provided valuable experience when he joined us from Toronto. I would also like to thank my advisor, Dr. Charles A. Barnes, for his support of this experiment.

Many people worked on this project at various stages. Dr. Jeffrey Ungar and Wuwell Liao worked on the prototype gas detector. Wuwell also generated the energy-loss and range tables for fractionally charged particles. Chris Wendt worked on the design of the high energy analysis system. Bruce Vogelaar worked on the construction of the full-scale gas detector. Jim Labrenz and Kevin Wilson ran shifts during the taking of data and also worked on data analysis. I would also like to thank Bob Carr and Murlin Price for their assistance. Finally I would like to thank Liz Wood for her help in typing this thesis.

Abstract

An ion-source and a charge spectrometer have been built which make it possible to search in solid stable matter for particles with non-integral charge. The ion-source uses a beam of magnetically analyzed 30 keV Ar^+ ions to sputter the sample in an ultra high vacuum environment. The charge spectrometer comprises a 3 MV Pelletron tandem accelerator followed by a 0.2% resolution electrostatic analysis system and a ΔE-E detector system. The entire apparatus has been constructed to be independent of mass over a mass range of 0.2 GeV/c^2 to 250 GeV/c^2. It is assumed that the fractionally charged particle is able to bind an electron.

A search has been carried out in samples of niobium and tungsten for fractionally charged particles (FCP) with fractional charge modulo 1/3. In particular, we have looked for $Z = N + 1/3$; N=0,1,... and $Z = N + 2/3$; N=0,1 . Upper limits have been obtained for the FCP concentration per target atom. These upper limits vary between 1×10^{-16} and 3×10^{-19} depending on the material searched and the charge state examined. Some interesting events have been seen. These are FCP candidates, but they can also be explained as improbable integrally charged events.

TABLE OF CONTENTS

TABLE OF CONTENTS (CONTD.)

List of Figures

List of Figures (cont.)

List of Tables

I. Introduction

A. Prologue

Electric charge is one of the fundamental quantities in nature. It is absolutely conserved, to the sensitivity obtained in the best experiments. It has been established experimentally, [Dylla and King 1973] ,that the fractional difference between the magnitude of the electron's charge and the proton's charge is of the order of, or less than 10^{-21}. This result supports the invariance of electric charge under Lorentz transformations. It is very important to know the basic unit of this fundamental quantity.

Previous to 1964, the standard view of the atom was that it comprised a nucleus containing Z protons and (A-Z) neutrons. The neutrons were charged neutral and the Z protons each had a charge equal in magnitude but opposite in sign to the charge on the electron. The nucleus provided an attractive potential in which Z orbital electrons were bound. Thus the entire atom was neutral and the basic unit of charge was the charge on the electron. This had been measured by Millikan in his famous oil-drop experiment in 1910, and the present value for the charge on the electron is

$$e = 1.602\ 189\ 2(46) \times 10^{-19}\ C.$$

However, in 1964, Gell-Mann, and independently, Zweig, postulated that all hadrons were composed of particles with charges $\pm 1/3$ or $\pm 2/3$ of the basic electronic charge [Gell-Mann 1964 ,Zweig 1964]. There were a number of factors which made this model plausible in the 1960's.

Firstly, electron-proton scattering had demonstrated that the proton had a finite form-factor. This meant that the proton had a finite charge and magnetic-moment distribution. Thus it was reasonable to postulate that the proton charge cloud was composed of some smaller constituents, just as the charge cloud of an atom was discovered to be a probability distribution of point electrons.

Secondly, experiments in the 1940's and 1950's had discovered a large new class of hadronic particles. These particles were classified by the "eightfold-way" SU3 symmetry of Gell-Mann and Neeman. This symmetry directly suggested the quark structure of Gell-Mann and Zweig.

The quark hypothesis was given additional support from the results of deep-inelastic scattering experiments of electrons on protons at SLAC in the late 1960's. The phenomenon of Bjorken scaling showed that the proton was composed of spin-$\frac{1}{2}$ pointlike objects.

Thus if the proton and all nuclei were composed of fractionally charged particles (FCP), it was obvious to an experimentalist that one should search for such objects in matter. From 1965 to 1977 there ensued many measurements all of which proved negative. These measurements have been summarized by Jones in his review article [Jones 1977] and I will here give a summary of the results.

The quark searches fall into three categories, namely cosmic-ray searches, accelerator searches and searches in stable matter. In cosmic-ray searches one obtains an upper bound for the flux of quarks. This is measured in several ways. For a quark with rest mass less than about 10 GeV, single-particle cosmic-ray searches are most sensitive. Typically this kind of search consists of layers of scintillator which allows one to measure $\frac{dE}{dx}$ of the incoming particle. The results are

for 1/3e $\qquad \varphi \leq 1.1 \times 10^{-11} (\text{cm}^2 \text{ sr sec})^{-1}$ (90% C. L.)

for 2/3e $\qquad \varphi \leq 2.4 \times 10^{-11} (\text{cm}^2 \text{ sr sec})^{-1}$ (90% C. L.).

If the mass of the quark is greater than 10 GeV, or if the production threshold is much higher, then they would most often be accompanied by a dense flux of shower particles. Hence people have looked in air showers. The upper limits obtained here are

for 1/3e $\qquad \varphi \leq 0.71 \times 10^{-11} (\text{cm}^2 \text{ sr sec})^{-1}$ (90% C. L.)

for 2/3e $\qquad \varphi \leq 1.4 \times 10^{-11} (\text{cm}^2 \text{ sr sec})^{-1}$ (90% C. L.).

Accelerator searches involve striking a target with a proton beam and looking with a detector for possible quark signatures. Most experiments employed a detector telescope of several scintillation counters in a secondary beam with pulse height analysis of each. Typical upper limit quark fluxes obtained were

$$\frac{d^2\sigma}{d\Omega dp} \sim 10^{-35} \, \text{cm}^2 \, \text{sr}^{-1} (\text{GeV}/c\,)^{-1}.$$

The third type of quark search is in stable matter. This experiment belongs to this category. Generally the search proceeds as follows. If an FCP combines with atomic matter, the resulting atom or molecule will not be electrically neutral and it should be possible to influence it with electric fields. This property of fractionally charged matter is the basis of several enrichment schemes. As an example, water may be boiled and the steam passed between a parallel-plate condenser. The electric field of the condenser would presumably drive the FCP onto the plates of the condenser. These plates could then be used in the source of an optical or mass spectrometer. However, the negative results obtained from experiments using such techniques can mean either that no quarks exist or that they do not behave in stable matter in the assumed way. If one restricts oneself to unenriched schemes, then the best number is from a ferromagnetic levitation experiment of Morpurgo's group [Gallinaro, et al., 1977]. They obtained an upper limit of 3×10^{-21} quarks per nucleon.

Such was the state of affairs until 1977 when, for the first time, a group reported a convincing observation of free fractionally charged particles (FCP). This was the group of Fairbank's at Stanford, and their experiment and its results are described in the following section.

B. Fairbank's experiment

This experiment is basically a superconducting version of Millikan's oil-drop experiment. It consists of a ball of mass $\sim 9 \times 10^{-5}$ g which oscillates vertically at a frequency of ~ 0.8 Hz in a magnetic field. The ball is levitated between two horizontal capacitor plates 15 cm in

diameter and with a gap of 1 cm. The position of the ball is sensed by a superconducting pickup coil coupled to a superconducting-interference-device magnetometer. The charge on the ball can be changed at will with moveable β^+ and β^- emitters. A 2 kV peak-to-peak square wave is applied to the plates in phase quadrature with respect to the oscillations of the ball. Every 50 cycles the phase of the square wave is reversed. The difference between the time rate of change of the envelope of the ball's oscillation before and after reversal is independent of the damping and proportional to the charge.

The results of Fairbank's group from 1977-81 [LaRue, et al., 1977, LaRue, et al., 1979, LaRue, et al., 1981ab] are shown in Fig. 1. The data, if correct, give clear evidence for the existence of fractional charges with the value of the fractional charge being modulo $1/3e$. There have been numerous discussions in the literature of both the experimental technique and the results, and the original interpretation of the experimental results as evidence for the existence of fractionally charged particles remains intact. It was this experiment of Fairbank's group which motivated the work described in this thesis. There are a number of conclusions which one can draw from this experiment which relate to the properties of the fractionally charged particles.

Firstly, Fairbank's group searched in two types of spheres, one of completely unannealed niobium, and the other of niobium annealed on a tungsten substrate at 1850°. This was done to improve the Q of the balls. It was only the annealed spheres which yielded positive FCP measurements. This could possibly mean that the FCP were present in the tungsten rather than the niobium. Hence for the first run of the present experiment, it was decided to search in both tungsten and niobium.

Secondly, there was strong evidence that the FCP were mobile. It was found that on certain balls the charges changed between levitations. During this time the balls contacted their plastic holders and the capacitor plates, but remained in the low-temperature environment. Also one ball, which had indicated the presence of an FCP, was scrubbed with

alcohol and when remeasured had zero charge. One possible interpretation of these observations is that the FCP are near the surface.

C. Experimental design goals

The object of the Caltech experiment was to search in solid stable matter with a sensitivity comparable to that of the Stanford group. The spheres used in the Stanford experiment had a mass typically of 90 μg and so contained 6×10^{17} atoms. If one assumed one FCP on each sphere, then the Stanford group was observing fractional charges in matter at a concentration of 1.7×10^{-18} FCP per niobium atom. Thus it was clear that the Caltech experiment had to demonstrate this level of sensitivity.

A second concern was that the experiment should be as mass-independent as possible. This was obviously necessary as the mass of these FCP was completely unknown. This entailed that all the optical focussing elements on the beamlines be electrostatic and not magnetic. There were three magnets permanently fixed in the system, the low-energy source inflection, terminal source inflection and high-energy analyzing magnets. These clearly had to be degaussed. As much of the beam-line as possible should be shielded in mu-metal. This was most important at the low-energy end of the machine, where the velocities of the particles were low.

Because of Fairbank's observation that the FCP seemed to be mobile, and hence probably on the surface, a technique which sampled the surface of a target would be clearly most sensitive. Thus it was decided to employ a sputtering technique to dismantle the sample. Clearly this would have to be done in a fashion which preferentially selected FCP. The assumption was that the FCP were present in the sample *ab initio* and the sputtering process caused them to be ejected from the bulk sample to a region where they could be swept away by an electric field. However, this sputtering process also generated secondary ions, and these would clearly give rise to a background in the experiment. Thus a magnetically

analyzed 30 keV Ar^+ beam was used to sputter the target in an ultra high vacuum environment. This sputtering by a noble gas in a clean vacuum would reduce the secondary ion yield.

It was also important to be able to search for both signs of FCP. Clearly the experiment requires negative injection into the tandem accelerator; thus, for positive extraction, charge exchange is necessary. This was important because, as will be discussed below, simple chemistry arguments indicate that certain particles will preferentially come off positive and others negative in the sputtering process.

D. The chemistry of fractionally charged particles

It must be stated initially that this experiment requires that an FCP be able to bind an electron. This is necessary because the operation of the tandem accelerator with its positive high voltage terminal requires that a negative ion be injected on its low energy injection end. This ion is then stripped in the terminal to a positively charged ion which is repelled to ground. This requirement is very reasonable if the FCP's long-range interaction is dominated by electromagnetism. The observation of Fairbank's group that the FCP are mobile would tend to support this contention.

It is possible for FCP to exist in two independent forms in matter. They may be found in isolation, i.e., unattached to either negative electrons or positive atomic nuclei. They could also be found in association with particular nuclei. This association could be either chemical or through a strong interaction bond. It is currently not known which nuclei these might be. Lackner and Zweig have investigated the chemistry of fractionally charged atoms and, in particular, have calculated the electronegativity and ionization potential for any such atom in the periodic table. They make two assumptions in their work. They assume that the mass of a free FCP is much greater than that of an electron. This is very reasonable if one makes the identification of an FCP as a quark, i.e., as one of the constituents of a nucleon. Secondly, they assume that the

nonelectromagnetic interaction of an FCP with nuclear matter is negligibly small at atomic distances. Although the nature of the strong interaction between FCP and nucleons is unknown, its associated length scale is presumably significantly less than the Bohr radius of an electron.

Thus we picture a fractionally charged atom as a central net positive charge of $N \pm 1/3$ or $N \pm 2/3$ with N orbital electrons. Because of the second assumption above, the size of the central charge is expected to be very much less than the Bohr orbit of an electron. Hence a fractionally charged atom has a small positively charged nuclear center surrounded by an electron cloud of conventional atomic dimensions. The interactions of this atom are thus governed by the familiar laws of chemistry. It is to be noted that Lackner and Zweig's analysis makes no other assumptions about the nature of the FCP. They could be quarks, diquarks, or more exotic objects such as hadronic colour singlets, leptons, or even quark constituents.

Lackner and Zweig's procedure is to determine the chemical properties of atoms with fractional nuclear charges $Z = N \pm 1/3$ and $Z = N \pm 2/3$, $N = 1,2,...$, by interpolating these properties within isoelectronic sequences, i.e., states with the same number of electrons but with different nuclear charge. Thus the chemistry of a fractionally charged atom (FCA) is described in terms of the known chemistry of the neutral atom $Z = N$, and the known chemistry of the ions $Z = N \pm 1$.

Consider FCA with $Z = N + 1/3$ and $Z = N + 2/3$, $N = 0,1,2, \cdots$. This covers all the possibilities as one may obtain $Z = N - 1/3$ and $Z = N - 2/3$ from $Z = N + 1/3$ and $Z = N + 2/3$. Recall that the electron affinity of an atom, EA, is the energy released by the addition of an electron to the atom. The work function φ of the sputtering surface is the energy required to remove an electron from the surface to infinity. Consider now a positively charged FCA present on the sputtering surface. It is possible for the FCA to come off positive but if the energetics are right, it may be more favorable for it to pick up an electron and come off negative. In the former case the

positive ion and electron come off separately, so the energy rquired is φ eV while in the latter case the energy released is EA eV. Thus if $EA \gtrsim \varphi$, the FCA will be likely to come off negatively charged, while if $EA \lesssim \varphi$, it will come off positively charged. Recall that the work functions for niobium and tungsten are, respectively, 4.33 eV and 4.56 eV. There is a further observation which gives information on how large the electron affinity must be for a large probability for negative ion formation. In this experiment, the major component of the direct negative extraction beam was chlorine and the observed current of 2 nA was consistent with 100% ionization and collection of the known chemical abundance of chlorine in the niobium sample. Now the electron affinity of chlorine is 3.5 eV, so it is reasonable to assume that all FCA with $EA > 3.5$ eV come off negatively charged. This is true for the entire periodic table for $Z = N + 2/3$ and for certain areas of the $Z = N + 1/3$ table.

The strategy for an FCP search is now clear. A direct negative extraction search should cover all the $Z = N + 2/3$ possibilities, and the indicated region above at $Z = N + 1/3$. A positive extraction search followed by charge exchange should be sensitive to those regions of the $Z = N + 1/3$ table not covered in the direct negative extraction search. However, the $Z = N + 2/3$ search is degenerate with the $-1 \rightarrow +2$ integral charge ion beam in the accelerator, and so only the charges $2/3$, $5/3$ with masses less than about 10 GeV/c^2 can be sought with significant sensitivity. The case $Z = N + 1/3$ can, however, be completely investigated.

II. Experimental apparatus

A. General overview

The purpose of the experiments described here is to search in samples of solid stable matter for evidence of fractional charged particles. In particular we look in pure metals for evidence of particles with charges $\pm 1/3$ or $\pm 2/3$. The basic principle of the experiment is to construct a sputter source which preferentially selects FCP over normal ions. This source injects in a mass-independent way into a tandem accelerator which acts as a charge filter. There follows a system of electrostatic analysis which selects particles with a given electrostatic rigidity (cf. Appendix A)

$$\frac{1}{R} = \frac{KE}{q}\frac{1}{V_T}$$

where KE is the kinetic energy, q is the charge, and V_T is the Pelletron terminal potential. The desired charged particle finally comes to rest in a detector which measures its energy. Hence the charge is well-determined. The basic layout of the experiment is shown in Fig.2.

The experiment could not have been designed without the use of two beam-optics codes. The extraction geometry and analysis system were designed with the aid of the SLAC Herrmannsfeldt program [Herrmannsfeldt 1979]. This program solved Poisson's equation in a general configuration of electric and magnetic fields under the constraints that the geometry have either a cylindrical or rectangular symmetry. The program used a finite difference method to solve the boundary value problem. For general beam transport calculations we used a code called TRANS, which was obtained from NEC. This program describes optical elements by two-dimensional matrices and is a first-order calculation of the trajectories. It follows the history of the phase-space ellipse as the beam traverses the optical system. We found the program useful for obtaining a first guess at the location of optical elements.

The system was designed to be mass-independent insofar as possible. This meant degaussing the source inflection, terminal inflection and analyzing magnets to the order of 0.5 gauss. Most of the accessible areas of the extractor and injector were shielded with high-permeability mu-metal. This reduced the magnetic field in the beamline to fields of the order of 0.2 gauss. The long drift region after the analysis system was similarly shielded. The requirement that the system be mass-independent meant that all the optical elements be electrostatic. This necessitated replacing the high energy quadrupole on the Pelletron, which was magnetic, with an electrostatic quadrupole.

Because the probability for charge-changing collisions in the residual gas of the beamline was proportional to the residual gas there, it was necessary that the vacuum be as good as possible. This meant that the beampipe and all optical and vacuum parts were made from 304 stainless steel and ceramic. Conflat flange hardware with copper gaskets was used throughout. Any copper used was oxygen-free high conductivity (OFHC). All the stainless steel pieces were pickled and passivated before installation.

B. Argon sputter source: principle

The goal is to design a source for extracting FCP from matter in such a way that they may be injected into, and accelerated by, a tandem accelerator. Although one could try to inject with standard negative ion sources, it is certain that this method would introduce very large background rates. Standard sources are designed to maximize integral ion yields and so inject a large amount of normal matter into the accelerator.

Rather, this experiment employs a sputtering technique in a clean ultra-high vacuum environment. One uses a sputtering beam, argon, which produces little ionization. One sputters at an energy of ~ 30keV as the sputter yield is large at this energy. Also the theory of the sputtering process at this energy is well understood [Sigmund 1969].

The sputtering yield. S, is defined as the number of target atoms emitted per incident ion. S for 30 keV Ar^+ on niobium is 6.3 and on OFHC copper is 11. The differential sputtering yield can be readily shown to have the following dependence

$$\frac{d^2S}{dEd\theta} \propto \left[\frac{dE}{dx}\right]_n \frac{\cos\theta}{E^2[1 + \frac{u}{E}]^3}$$

where θ is the angle with respect to the normal to the surface which the emitted particle makes; $\left[\dfrac{dE}{dx}\right]_n$ is the nuclear stopping power as given by Lindhard, et al., 1968; u is the surface binding energy, which is of the order of 1 eV. There are some important points to note about this result.

It is clear that there is an energy distribution of sputtered secondary atoms. However, this distribution is peaked at half the surface binding energy ($\sim$ 1 eV) and falls off like E^{-2} for $E \gg u$. This effect is important when one comes to calculate the emittance of the source. Secondly, one can see that the emitted ions will be forward peaked. This is clearly advantageous as it reduces the emittance. Finally, we see that the sputter yield is directly proportional to the nuclear stopping power.

This analysis is for sputtered atoms. The secondary ion yields in this experiment are experimentally found to be of order 10^{-4}. There exists no coherent theory of how secondary ions are formed on surfaces.

C. Argon sputter source: hardware

The purpose of the argon source is to produce a beam of approximately 30 microamps of magnetically analyzed 30 keV Ar^+ on a 1mm spot in an ultra high vacuum environment. The general layout of the source is given in Fig. 3. The Ar^+ is produced in a General Ionex [hereafter abbreviated to G.I.] model 358 duoplasmatron. The filament is a platinum gauze which is coated with a solution of $CaCO_3$, $SrCO_3$, and $BaCO_3$ and allowed to dry. The filament is then outgassed over a period of approximately eight hours during which time the carbonates are converted to oxides and CO_2

is liberated. Beam is extracted at + 30 kV from the head, so all the electronics associated with the source [extractor, filament current, filament bias, magnet current supplies] must be at + 30 kV with respect to the remainder of the source. These electronics are located on a stand, which we shall call stand 1, and whose potential we shall denote by HV1.

For this discussion, refer to Fig. 3. After extraction the beam is collected by L1 and basically parallel transported to L2. The L1 power supply is at potential HV1. Between L1 and L2 is an inline valve which allows one to isolate the duoplasmatron head from the remainder of the vacuum system. This is convenient when the filament needs to be recoated or the head needs cleaning. Einzel lens 2 is located inside the cryo torr 8 (CT-8) pump tee and is a 3" aperture lens. The CT-8 pump has a pumping speed of 1200 l/s for argon and is run at a static helium pressure of 250 psi. Its compressor is located at ground potential and so the helium lines must be insulating. The lines are Aeroquip model FC370-06 insulating lines. These lines require that the pump be regenerated and the helium flushed approximately every 5 days. The purpose of Einzel lens L2 is to produce a waist at the 1/8" Cu aperture. This aperture is cooled by liquid freon 113.

Directly in front of the aperture is the 30° bend. The purpose of this is to analyze the argon beam and ensure that none of the customary contaminants found in a duoplasmatron is actually present in the beam which sputters. The presence of even small quantities of, e.g., oxygen or chlorine would give rise to large secondary ion yields and hence present a large background for the experiment. The radius of the magnet is 9" and the magnet box is a 1" o.d. cylindrical pipe. This requires 3.8 kgauss and 12 A of current. The magnet is cooled by liquid freon 113. A 1 cm diameter cold trap, 18" in length, follows the aperture. The purpose of this trap is to isolate the Ar gas load at the duoplasmatron head from the ultra high vacuum target chamber. When running ,the typical pressure read on IG1 is 2×10^{-5} torr. Under these conditions, it is necessary to top up the cold-trap at least every 12 hours. The cold-trap is followed by an inline valve which is used to isolate the uhv target chamber from the remainder of the vacuum system. It enables one to change targets in the chamber

without warming up the CT-8 cryo pump.

Einzel lens 3 follows the valve. The purpose of this lens is to take the approximately 1/4" dia Ar^+ beam and focus it onto a 1 mm spot on target.

The target chamber and extraction geometry are shown in Fig. 4. It is seen that the incoming beam passes through a 1mm diameter hole in the copper extractor plate. After several days of running beam, this hole becomes enlarged because of constant sputtering and so one needs to replace the extractor plate if more running on this target position is desired.

The target ladder is constructed as follows. The manipulator is made of 304 stainless steel. The vacuum feedthrough is in the form of a welded bellows. The thread mechanism is brass on stainless steel, with the feed being twenty threads per inch. The manipulator is mounted on a 3.5" o.d. conflat flange. There is a copper piece electron beam welded to the stainless steel. This serves as a good thermal conductor to conduct heat away. The heat load at the sputtering site is calculated to be 1 watt. The copper block is cooled by freon 113 cooling lines which come from outside the vacuum system down the center of the manipulator. This part of the target holder is at HV2 potential. However, the targets require a bias of 10 kV in order to extract the secondary ions formed. Thus mounted on the copper block is a layer of 0.125" thick macor. On top of this, in electrical isolation from the body of the target holder, is another layer of copper on which are directly mounted the targets to be sputtered. On this copper layer are machined with close tolerances, recesses into which the targets snugly fit. These targets are 1.125" x 0.5" x .063" rectangular copper pieces. The material to be sputtered is positioned in the center of one of these copper pieces. Thus for niobium and tungsten targets, we press fit a 0.25" diameter disc into the copper. The target holder has positions for five targets. However, the center position has a 0.375" diameter hole drilled right through and this position is used for tuning up the argon beam, cf. Fig. 4.

Targets are changed by removing the top 10" diameter flange on the target chamber. The complete manipulator mechanism is fixed to this removable flange. The alignment of the target holder is fixed by scribe marks both on the top flange and on the side of the target chamber. These scribe marks were determined initially by sighting on the target ladder with an external telescope and demanding both that the plane of the targets be perpendicular to the direction of extracted beam, and that the centers of the targets be aligned with the extraction optics.

The extractor plate is mounted off the target holder and is also at HV2 potential. It consists of five 0.5 cm diameter extractor holes with corresponding 1 mm diameter holes drilled at 45° with respect to the normal to the surface of the target. The 1 mm hole is where the 30 keV Ar^+ beam enters. The location of these 1 mm holes must take into account the fact that the 10 kV target bias will affect the trajectory of the 30 keV Ar^+ beam as it approaches the sputtering site. Thus the extractor plate design is a function of the sign of the extracted particles, the target bias and the Ar^+ beam energy.

The center target position has a 1/4" diameter hole which allows the beam to pass right through the target holder where it enters a Faraday cup. This permits one to tune up the beam and verify that there are 30 μA of 30 keV Ar^+ passing through a 1 mm diameter hole. Beneath the target chamber is a CT-7 cryo pump. This pump has a pumping speed of 850 l/s for argon. Like the CT-8 pump, when running, the CT-7 resides at high voltage so it uses identical insulating lines to the CT-8. It shares a compressor with the injector cryo pump, which is another CT-7. The base pressure in the chamber is 5×10^{-9} torr, but when running is typically 7×10^{-8} torr. This pressure is read on the nude ion gauge IG2, whose location is shown in Fig. 4.

D. Extraction and Injection

The Ar sputter source produces a 30 μA 30 keV Ar$^+$ beam on a 1 mm diameter spot, so one must now collect all secondary ions produced at the sputtering site, accelerate them across 70 kV potential and inject them into the pelletron. The extraction geometry is shown in Fig. 5a. It was designed using the Herrmannsfeldt SLAC program and is modeled on the extraction design used in the KAMEKA ion probe. Some of the output rays generated by this code are shown in Fig. 5a. The extraction gap and aperture can be viewed as a combination of uniform acceleration and a divergent gap lens. Consider now the schematic of the extraction geometry as illustrated in Fig. 5b. The target T is at potential V with respect to the extractor E. Let the beam spot size be 2c and the maximum emitted sputtered energy be φ_0. d is the distance between the target and the extractor. We can view the process as follows:

(i)   Uniform acceleration between T and E

We can write expressions for the maximum extent and maximum angular divergence, respectively, as

$$x_{max} = c + 2d \sqrt{\frac{\varphi_0}{V}}$$

$$\theta_{max} = \sqrt{\frac{\varphi_0}{V}}.$$

(ii)   At the extractor E we have a divergent gap-lens with focal length

$$f = \frac{4 \varphi_0}{E_2 - E_1}$$

where E_1 and E_2 are the values of the electric field on either side of the extractor plate [cf. Zworykin, et al., p. 445].

Thus we can write for the maximum angular divergence

$$\Delta\theta_{max} \approx \frac{c}{4d} + \frac{1}{2} \sqrt{\frac{\varphi_0}{V}}.$$

We can thus write for the total emittance of the source

$$\varepsilon = \pi \left\{ c + 2d \sqrt{\frac{\varphi_0}{V}} \right\} \left\{ \frac{c}{4d} + 3/2 \sqrt{\frac{\varphi_0}{V}} \right\} \sqrt{V} \sim \pi \, 5000 \text{ mm mrad} \sqrt{eV} \, .$$

This value of the emittance is close to the value quoted for the standard Middleton sputter source. This value of emittance is inserted into the beam-optics code TRANS and the behavior of the beam traced through the complete experiment. In turn, one designs other optical elements based on the value of this emittance. One can predict the size of the beam at all positions along the beamline and in general there was satisfactory agreement between what was predicted and what was observed.

The general layout of the injector system is given in Fig. 6. The extractor einzel lens [see Fig. 4] collects the extracted beam and transmits it to the 15° electrostatic analyzer. This analyzer was designed so that there is no line of sight between the rubidium charge exchange canal which follows and the targets on the target ladder. This is to prevent deposition of rubidium on the surface of the sputtering target. Such a deposition, of course, would lead to enhanced ion yields. The 15° analyzer has a radius of 11.5" and a gap of 3/4". After the analyzer is the rubidium charge exchange canal. This is used only for direct positive extraction. It was built by National Electrostatics Corporation (NEC). The temperature of the canal is controlled by a temperature controller, which is connected to both the heating element and a thermocouple. The optimum temperature for the canal was found to be 175°C, as measured by the thermocouple.

For direct negative extraction, the target bias, extractor lens and 15° electrostatic analyzer are tuned for negative particles. For positive extraction followed by charge exchange, these three elements are tuned for positive particles. This means that the polarities of the target bias and extractor lens must be reversed for positive extraction. Also the polarity of the 15° analyzer must be reversed.

Then follows the accelerating column. This is an NEC-built accelerating column and is rated for 70 kV. All electronics before this column and after the 2490 G.I.einzel lens are located at potential HV2. Thus at HV2 we have the 30 degree magnet supply, L2 supply, L3 supply, target bias supply, extractor lens supply, 15 degree esa supply, IG1 controller, IG2 controller.

The accelerating column acts as a sharply focusing lens which produces a waist mid-way between it and the injector lens. The injector lens is a 2.5'' diameter lens. This is followed by a cylindrical 30° electrostatic analyzer of radius 4' and length 2' which steers the beam into the pelletron. The plates in this analyzer were machined using a computer controlled milling machine. This electrostatic analysis serves in conjunction with the charge exchange canal as a charge filter for positive extraction measurements.

The total injector bias is given by the sum of the target bias and the table bias. These potentials were 8 and 70 kV, respectively. Thus an integral negative ion would have energy 78 keV. A directly extracted - 2/3 particle would have energy 52 keV. A directly extracted - 1/3 particle would have energy 26 keV.

It should be added that there was a 50% loss in transmission between the injector cup and the LE cup. This was probably due to a large beam size at the 30° cylindrical analyzer. This factor was taken into account in all FCP concentration calculations.

E. Pelletron

The pelletron is a 3MV machine manufactured by National Electrostatics Corporation . One relevant parameter for this experiment is that its voltage stability on generating voltmeter (GVM) regulation is $\sim 1:10^4$. The GVM was calibrated at 496 kV by means of the 992 keV resonance in the $^{28}Al(p,\gamma)$ reaction. The type of stripper used in this experiment is a gas stripper (both H_2 and N_2) pumped by titanium sublimator pumps , one on each side of the stripper canal. At each end of the machine are

Sargent-Welch turbo pumps. The base pressure at each turbo is $\sim 3 \times 10^{-8}$ torr. When the stripper is run for maximum H^- transmission, the pressures over the turbos become $\sim 2 \times 10^{-7}$ torr. The stripper is designed so that the stripper gas is pumped symmetrically. For optimum transmission through the machine, good terminal pumping was important. This meant that the terminal sublimators had to be outgassed for about 40 minutes at the beginning of each run.

The pelletron ran comfortably at 3 MV. However, the value of the terminal potential for this experiment was determined by two constraints. The transmission of the machine was better at 2 MV than at 3 MV. This was because of the energy dependence of the stripping cross sections. As one went to lower energies, however, the FCP pulse height window, because of the pulse height defect phenomenon, was shifting into the large low energy background. Thus the compromise value of 2 MV was chosen for the $R = 1/3$ measurements. The $R = 2/3$ run had a 3.4 mgcm^{-2} aluminum window and so, to increase the stopping powers of the particles, we ran at 3 MV.

The transmission of the machine was investigated using the G.I. sputter source. The transmission from the low energy cup to the object cup for hydrogen with 2 MV on terminal was regularly about 75%. Of this about two-thirds was transmitted to the FCP detector station. Thus the total transmission from low energy cup to detector for 4 MeV hydrogen was 50%. Between a proton mass and an oxygen mass, the +1 transmission from low energy cup to FCP detector station for 4 MeV particles was about 20%. Above mass 20 amu the +1 transmission was found to be flat and of the order of 5%. The transmission for the direct extraction FCP source, which was known to be 85% chlorine, was found to be 12%. This was the number which was used in obtaining quoted sensitivities for all masses above 10 $\frac{GeV}{c^2}$. The charge state fractions were measured and reasonable agreement was obtained with the standard Gaussian charge state distribution [Wittkower, 1971].

For lightly ionizing particles, the stripper used was N_2. For heavily ionizing particles, however, the gas used was H_2. This reduced multiple scattering effects and increased the charge-state +1 fraction.

F. Analysis system

The electrostatic analysis system was designed to have a resolution of $\sim 0.2\%$ for 2 MeV ions. The resolution of an electrostatic system is defined in Appendix A. The layout is shown in Fig. 7. There are two distinct sections. The first section comprises a single set of parallel plates while the second has two sets of plates. It comprises 3" tall 304 stainless steel plates 30 cm in length. For 2 MeV ions the effective length is 32 cm. It is designed so that the beam stays as far away from the plates as possible. The system is designed so that the entire system operates on one set of power supplies. For $R = 1/3$ at 2 MV the voltage between the plates is typically 25 kV. The voltage is balanced so that there is zero potential midway between the plates. This system was designed with the aid of the Herrmannsfeldt program mentioned above. The base pressure is typically 5×10^{-8} torr in the region of the plates.

The system is designed so that when tuned for $R = 1/3$, then the $R = 1/2$, $2/3$, etc. beams do not get past the variable horizontal slit S2. The fixed slit F1 between the two sets in the second stage of analysis has the function of eliminating any halo which would hit the plates. This slit also puts a vertical limitation of $3/4''$ on the beam. To define a high resolution for the second stage of analysis one positions the variable slit S3 just after this stage. Further down the beamline we have another fixed collimator F2 to eliminate any possible scattering from the inside of the beam-pipe. The inclusion of F1 and F2 was determined by experiment, and it resulted in a large decrease in the background in the experiment. The settings for the object slits S1 and horizontal slits S2 and S3 are obtained using known mass beams (e.g. H, O, Cu...) from the G.I. source, and demanding that all particles with masses greater than 200 MeV/c^2 be transmitted through the system

Important to the operation of the experiment is the computer control of the high energy quadrupoles and electrostatic analysis system. This is set up in a very similar way to the data acquisition system. One of the LSI-11 satellites is dedicated to the task. It talks to a CAMAC crate which has a display driver, scanning digital voltmeter (DVM) and digital to analog converter (DAC). The high voltage is generated by Glassman high voltage supplies which are 0-10 V programmable and have a 0-10 V readout. The DVM measures the voltage output and the DAC talks to the program inputs on the supplies. The display driver displays the present values of the voltages on a TV monitor. Also there is a toggle switch on the control box which enables one to disable the computer control and locally control the high voltage supplies using ten turn potentiometers. This computer control system was vital to the success of the experiment as it enabled the easy scaling from one charge state to another. All values could be stored in the computer. One typically had $R = 1/2$, $R = 1/3$ and FCP settings stored in memory and could go from one to the other as desired.

G. Detector

The detector station is shown in Fig. 8. The two different parts to the experiment, i.e., low mass, N_2 stripper and high mass H_2 stripper, demanded two different detector stations. For high mass searches we used a heavy-ion high electric field, thin junction type of Si detector [D1]. This was mounted on a Huntington manipulator. The manipulator had a sheet of tantalum with two identical 1/4" diameter holes 1.5" apart. One hole represented a real collimator for the beam while the second had the silicon detector mounted behind it. To tune all beams for the low-mass search and to verify mass independence , the collimator was positioned in the beam path. Thus one verified that all the beam travelled through the 1/4" diameter hole. To take data, the Si-detector was then positioned in the beam path and one was sure that one was not losing beam.

The type of detector used was a Tennelec detector model number HI-100-60-25-EM. It had an active area of 100 mm^2 and a sensitive depth

of ≥60 microns at a bias of +100 V. It was found that the major source of background in the region of interest, i.e., 0.5 - 3.0 MeV was from room gamma-rays interacting in the depletion region. This was deduced from the following evidence. When the applied bias was lowered, the background dropped. Of course, lowering the bias decreases the depletion depth which lowers the total volume of interaction. Also it increases the capacitance which would increase electronic noise. Thus clearly electronic noise was not the origin of the background. The other clue was that bringing a ^{60}Co source near the detector increased the background and, conversely, shielding with lead lowered the background. Based on these considerations we ran at a bias of +33 V and surrounded the cross with 2" of lead shielding. This resulted in 1 background count every 4 hours in the region from 0.6 to 2.1 MeV.

For the low mass N_2 stripper search we used the setup behind the detector Faraday cup, as illustrated in Fig. 8. This will hereafter be referred to as D2. This consists of a gas ΔE detector followed by a 500μm Si-detector followed by a 60 μm partially depleted detector. It is 30 cm in length and the gas used was isobutane $[C_4H_{10}]$. The window used was 20 μgcm^{-2} of formvar and was constructed of three layers, each 6μgcm^{-2} thick. The formvar was present in a solution of cyclohexanone. Each 6μgcm^{-2} layer was made by floating the formvar solution on distilled water and picking up the film with a rectangular piece of aluminum sheet which had a 3/4" diameter hole on it. The film was then laid on top of the window holder and allowed to dry before putting on the next layer. The thickness of the window was measured using the 5.486 α-line of ^{241}Am.

The gas ΔE detector was a gridded ionization chamber. The Frisch grid was constructed from 20 micron gold-plated tungsten wire mounted on a brass frame. The anode was run at +300 V and the grid at +150 V. These values were obtained by constructing plateau curves of pulse height as a function of both anode and grid voltages. The gas system was configured so that there was a steady flow of isobutane through the detector. The detector was operated at a pressure of 4" H_2O.

The E detector was mounted as indicated in Fig. 8 in the volume of the gas detector. It was a 500 μm totally depleted Si surface barrier detector, hereafter called Si1. It had an applied bias of +110 V. All known stable particles would stop in the GAS or Si1. However, certain classes of observable FCP could penetrate both and to detect these a third detector hereafter called Si2 was placed after the GAS and Si1 detectors. It was mounted as shown in Fig. 8. It was a 60 μm partially depleted silicon detector with an applied bias of +50 V.

The main source of background in the GAS-Si1-Si2 detector system is the interaction of cosmic rays in the 500 μm thick deplection region in the Si1 detector. One can calculate from geometric considerations and from knowing that the minimum ionizing peak for cosmic-ray muons in silicon is 1.62 MeV/(g/cm^2), that the peak of the Landau distribution is at approximately 200 keV. If one sets up the silicon surface barrier detector in the overlap region of two plastic scintillator paddles and demands coincidence between the events in the paddles and in the silicon detector, one obtains the spectrum shown in Fig. 9. One determines the peak to be at ~230 keV. This is in good agreement with the calculated value. It is the high energy tail of this distribution which gives rise to the background. It is clear then that to obtain good limits one needs to construct a cosmic-ray veto around Si2. Indeed, this is what was done. The gas detector was surrounded on four sides by 1/4" thick plastic scintillator paddles. The outputs of the bases were fed into a discriminator box with threshold at 30 mV. The gain of the paddles was set using the approx. 1 MeV Compton edge of the ^{60}Co source and the gain was set so that the discriminator threshold lay at about 100 keV. The addition of the cosmic-veto reduced the cosmic ray induced event rate from ~1 per minute to ~1 per hour.

H. Detector electronics

The data were accumulated on one of the satellites of the Kellogg data acquistion system. This is configured so that a VAX 11/750 mainframe communicates with several LSI-11 satellites. These LSI-11s each in turn controls a CAMAC crate. In the data acquistion satellite in our

experiment we had an ORTEC AD811 ADC and a Bi Ra Systems NIM IN module in the crate. The electronics setup is shown schematically in Fig. 10.

The GAS, Si1, and Si2 signals each are fed into a 142A preamp. For the silicon detectors the input impedance is 10 MΩ while for the GAS detector it is 1 MΩ. This is because of the lower intrinsic impedance of the silicon detectors. For these detectors also the energy signal is taken from the E output of the 142A and amplified by a 571 ORTEC amplifier. The gas signal is also taken from the E output of the 142A and fed through a Canberra 1413 amplifier. All these energy signals are sent via patch cable to the ADC.

Timing signals are taken from both the GAS and Si1 detectors. They are generated by teeing off the E output from the 142A preamp and feeding into a 474 timing filter amplifier. The silicon signal is not shaped but the GAS signal is integrated and differentiated with a time constant of 500 ns. Both signals are discriminated and fed into a 365 logic box. The signals may be ORed and ANDed here depending on the logic function desired. The output is fed into a 222 gate and delay generator and a 10 μs NIM pulse is generated which is used to strobe the ADC.

Now we must also address the question of vetoing the cosmic ray events is Si1. This is done using the NIM IN module. This is a twelve bit register. A strobe is required to update the register. In this application just bit 1 of the twelve is used. The output of the Si1 timing discriminator is delayed by a 222 and another discrimiator. This signal is then used to strobe the NIM IN module. Bit 1 is generated from the paddles as follows. The output of the phototubes is discriminated and four signals are fed into the 365 logic box where they are ORed. The output is then fed through a 222 whose NIM is fed into bit 1 of the NIM IN module. Thus every time Si1 gets an event it strobes both the ADC and the NIM IN modules. If bit 1 of the NIM IN is logic 1 then this is regarded in software as being a coincidence between Si1 and the paddles.

It was found during the initial stages of the experiment that the electronics was sensitive to pickup from the operation of certain switches. This was discovered to be partly due to poor electrical grounding in the lab as a whole. Thus it was decided to install a "glitch rejector." This is a Canberra pre-amp which has several feet of cable as an input and is placed near the detector pre-amp. The output is amplified, discriminated and fed into a 222, the TTL output of which is fed into a given channel of ADC. This TTL signal has a width of 10ms. Thus this will fire every time a glitch appears on the line. Then it is set up so that in software the ADC is shut off for 10 ms. The TFA gain is set so that the glitch rejector fires at about 1-3 Hz.

III. Experimental method

This chapter is devoted to a description of the procedures followed in setting up and executing the experiment. Generally, several days were set aside at the beginning of each run to set up electronics, prepare windows for the gas detector, overhaul the Ar sputter source and degauss all magnets.

A. Argon sputter source

At the beginning of each run it is found necessary in the interests of optimum extracted beam, to carry out the following procedure. The duoplasmation head is removed and thoroughly cleaned. In the process of outgassing, a residue develops on the walls of the zwischen and this is removed with emery paper and the zwischen then rubbed clean with methanol. The 10 mil aperture is cleaned and checked for no erosion. Once, during a loss of cooling to the anode plate, this aperture was completely eroded. Also the platinum gauze filament is cleaned in a dilute solution of nitric acid and recoated. The whole head is then reassembled carefully using the alignment jig. Then the head system is roughed out and opened to the CT-8.

Next it is necessary to outgas the filament. This means that the filament current is slowly raised from zero to its operating value of 30 A. During this process the bypass valve is open, to increase pumping speed. When the outgassing procedure is complete, the bypass valve is closed. Then Argon gas is introduced through the needle valve and the filament bias is turned on. At this point the arc should strike. Now a plasma exists and so beam may be extracted. Thus the grounding strap is removed from stand 1. Then the extractor supply is raised to ∼ 28 kV and L1 to ∼ 4 kV. The lollipop is now moved into the path of the beam and +300 V bias placed on it. Tuning the 30° magnet for the correct ridgidity should yield a beam current of 300-500 μA on the lollipop. To achieve this it is necessary to fine-tune all parameters but especially the source magnet current and the gas flow.

We are now ready to transmit beam through to the Faraday cup at the rear of the target chamber. To do this it is necessary that the target holder be in its center position where it has a .25" hole through it. Thus the 30° magnet is detuned, the lollipop removed from the beam-path and grounded and the 30° magnet retuned. Then by fine-tuning L1, L2, and L3 and the horizontal and vertical magnetic steerers it should be possible to obtain 30 μA of beam through the 1 mm diameter hole in the extractor plate to the Faraday cup.

At this point 30 μA of Ar$^+$ in a 1 mm dia. spot is ready to be placed on a target. Thus the target holder is moved so that the beam impinges on one of the four possible target positions. At this point all grounding straps from the stand are removed. A final check to see that the stand is floating is to bring a ground strap within a couple of mm of it. Some sparks should result as the stand discharges. Then -70 kV is applied to the stand. By fine-tuning the target bias, extractor lens, 15° esa, injector lens and 30° esa, it should be possible to obtain a couple of nanoamps of negative beam on the LE Faraday cup of the pelletron. One is now extracting and accelerating negative ions generated by the sputtering of the target by the 1 mm dia 30 μA Ar$^+$ beam. At this point it is necessary to fine-tune the controls on the argon line as well as those just mentioned. The total injection energy of the particles is the sum of the target bias and stand bias, and was typically 78 keV. This value was chosen to optimize transmission through the Pelletron.

When the sputter beam was placed on the target initially, the secondary ion beam could be as high as 40 nA but as the surface gradually cleaned up this would drop to 2-3 nA in about 1 hour. It should also be mentioned that there was a 50% drop in transmission around the 30° esa. This was due to the fact that the beam was larger than the plate separation (1 inch). One hundred percent transmission could certainly be achieved with some work but the resulting increase in sensitivity was not sufficient to warrant this at this time. This loss in transmission is included in all sensitivity estimations.

B. Detector calibration

The silicon detectors were calibrated using the 5.486 MeV α-particle emitted by Am-241. The α-source was mounted at the end of a moveable copper rod. The gain of the amplifiers is set so that the conversion between channel number and energy is 5 keV per channel. This number is the same for all spectra.

The gas detector had to be gainmatched with the silicon detector. This was achieved as follows. First, with the formvar window in, the silicon detector gain was set so that the α-peak was at channel 1097 (i.e., 5 keV per channel). Then the formvar window was removed and the shift in the α-peak gave the window thickness. Finally, the window was replaced and the gas detector pressurized to a pressure of 4" H_2O with isobutane gas. Then the gain of the gas detector was adjusted so that the sum of the GAS and Si1 detectors put the 5.486 peak at channel 1097. Then the gains of the GAS and silicon detectors were the same.

Another important concern was the location of the trigger threshold. This was determined by the TFA gains of the GAS and Si1 detectors. It was important that the thresholds be set so that one was triggering below at least 500 keV. This was necessary because it was possible to obtain pulses at about 600 keV from pulse-height defected heavy ions. The threshold was set using a pulser.

As mentioned earlier the gains of the paddles were set so that the threshold was at about 100 keV. This was done using the Compton edge of the ^{60}Co source.

Timing was another important consideration in setting up the detector. Firstly, one had to ensure that the width of the ADC strobe was sufficient to guarantee that both the gas and silicon pulses fell within this window. This was checked as follows. The α-source was directed at the GAS-Si1 detector. Then, triggering only on the GAS, one checked that the Si1 pulse was well within the strobe width. Conversely, triggering only on Si1, one checked that the GAS pulse was well within the strobe width. A 10 μs wide strobe was found to be adequate at all times.

The other timing consideration was that of the paddles with respect to Si1. The paddles were used to veto cosmic-rays in Si1, so one had to ensure that the pulse from the paddles fell within the strobe generated by Si1. This was done by setting Si1 up in a black-box in the overlap region of two plastic scintillator paddles. One used cosmic rays to generate pulses in both the paddles and in Si1. One demanded coincidence between both the paddles and Si1. One looked at this on an oscilloscope by triggering on the NIM IN strobe and looking at the paddle output. The rate was about 1 per minute. The strobe width was typically 200 ns.

For the rates encountered in this experiment, the dead-time was not a problem. It was typically less than 1%.

C. Mass-independence and tune of the system for direct negative extraction

(i) $R = 1/3$

Initially we shall consider the situation for $R = 1/3$; i.e., one is looking for FCP that enter the Pelletron with charge $-2/3$ and strip to $+1/3$ in the terminal. The procedure is the following. Firstly, the high energy analyzing magnet was degaussed using a bucking coil. Then the G.I. source was used to generate beams of H, O, Cu. This was done by using a copper pellet. This pellet was drilled and titanium hydride powder was packed into the hole. Typically, the beams were several microamperes in intensity. One was careful to arrange that the injection energy for the G.I. source was identical to that used with the FCP sputter source. The high energy analysis system and quads were tuned for $R = 1/2$. The copper beam was first tuned up and with the high-energy magnetic steerers off, the electrostatic analyzer and the high energy quadrupole were adjusted so that the copper beam ended up in the detector Faraday cup with maximum transmission through the machine, and optimum beam quality. The beam profile was observed on the detector station beam profile monitor. Then the hydrogen beam was tuned up and the high energy magnetic steerers adjusted so that the hydrogen beam ended up

in exactly the same place. The complete analysis of the particle kinematics for this procedure is discussed in Appendix A. It is to be appreciated that this is the only place in the entire experiment where magnetic fields are used to affect the beam. Elsewhere, every possible effort was made to eliminate stray fields. Sometimes it was necessary to iterate this procedure to converge to a unique tune. The oxygen beam was a further check on the tune. One now had a system mass-independent for masses between 1 GeV/c^2 and $\sim$ 65 GeV/c^2 at 4 MeV energy. One next had to ensure this mass independence from 200 MeV/c^2 to $\sim$ 200 GeV/c^2 for 2 MeV particles. This was achieved as follows. One determined at each of the three variable slit positions - object, S2 and S3 - the positions in space of the three beams, H, O, Cu. Knowing this we can calculate where a beam of arbitrary mass would lie, so the slits were set for a lower mass of 200 MeV/c^2 The difference in slit position between 200 and 64 GeV/c^2 was insignificant. One now had a system which was mass- independent down to 200 MeV/c^2. One then determined settings for $R = 1/2$, $2/3$. These were stored in the computer.

The G.I. source was now shut down and the low energy inflection magnet degaussed. The Ar source was tuned up as discussed above and tuned through the machine onto the detector station Faraday cup. Only very slight retuning from the G. I. tune was necessary to do this. One then had an $R = 1/2$ beam from the FCP source on the Faraday cup. Now one of the components of our negative extracted beam was hydrogen, which was very fortuitous in that it gave us an immediate means of checking the mass independence of our system from sputtering site, where the H$^-$ were made, to the Si1 detector, where they came to rest. So with an $R = 1/2$ beam tuned up, the desire was to put it on the detector. The typical intensity was several hundred picoamps which was too large and would destroy the silicon detector (we killed several this way). Thus it was necessary to detune the Ar beam. This was done by setting L2 and L3 to zero. To obtain good transmission for H, it was necessary to run the N_2 stripper at a meter reading on the Pelletron console of about 15%. One put the Si1 signal on an oscilloscope or ratemeter and then took out the

FCP cup. At this point one generally observed some rate from hydrogen particles in the silicon detector. One first checked the tune on the electrostatic analysis system by varying the energy of the beam by changing the terminal reference knob on the machine. Then one tuned the degauss on the low energy inflection magnet to maximize the rate. Finally, one tuned the high energy magnetic steerers. One now had verified the mass independence of particles extracted from the FCP source.

Next one scaled the quads and electrostatic analyzer settings by 1.5 from $R = 1/2$ to $R = 1/3$. One put this on the detector with the FCP source detuned and observed the rate of the $-1 \rightarrow +2 \rightarrow +1$ background beam. One checked the ESA tune again by changing the terminal energy and adjusted accordingly. Finally, one scaled by 1.013 to go from $R = 1/3$ to the FCP setting. One was now ready to take data.

It is worth noting that the quads did not exactly scale between charge states and this deviation increased at higher charge states. This effect was caused by the charge state dependence of the focussing effect of the high energy accelerating column. It was not large enough at low charge states to be of consequence in this experiment.

(ii) $R = 2/3$

Consider now the situation for $R = 2/3$. This experiment was run with 3 MV on terminal for reasons to be discussed below. Here one is looking for FCP that enter the Pelletron with charge - $1/3$, and strip to charge + $2/3$ in the terminal. These particles are degenerate in R-space with integral ions which are injected with charge -1 and strip to +2 in the terminal. There is typically a beam current of $\sim$ 100 pA on the Faraday cup at the FCP detector station. It is clearly impossible to put 10^8 particles/sec on the detector. Hence, in general, it is impossible to search for FCP at $R = 2/3$. One possible way of looking for these $Z = N + 2/3$ particles is to look for two-electron ($R = 5/6$) or three-electron ($R = 8/9$) stripping of the - $1/3$ particles. However, again

these FCP processes are degenerate, with $-1 \rightarrow +5$ and $-1 \rightarrow +8$ integral charge-change processes, respectively. The backgrounds are large in the $R = 5/6$ case. In the $R = 8/9$ case, it was not possible to scale reliably to the +8 charge state.

The strategy adopted was to place a 3.4 $mgcm^{-2}$ aluminum foil on the window of the gas detector. This foil stopped 6 MeV ions whose mass was greater than lithium. It made it possible to search for $Z = N +2/3$ FCP with N = 0,1 for all masses less than $\sim 10GeV/c^2$. The addition of the aluminum foil was the reason the $R = 2/3$ search was run with 3 MV on terminal. Higher terminal energy meant higher incident energy on the detector for a given charge state. This, in turn, implied a larger range in the detectable FCP mass range. This question is discussed further in the chapter on Experimental Results.

The mass-independence for the $R = 2/3$ search was set up as in the $R = 1/3$ case, using the G.I. source. Then, the FCP source was tuned at $R = 1/2$, and the fine-tuning of HE magnetic steerers and all degauss supplies done with the 6 MeV proton beam. The slits were set for all masses greater than 200 MeV/c^2 as above. The HE optics were then scaled to the +2 charge state, and the $\sim$ 100 pA beam fine-tuned on the FCP detector station cup. One was then ready to take data.

In the course of the experiment, the data acquisition was halted every hour. The $R = 1/2$ mass-independence procedure and the $R = 1/3$ voltage setting were checked. This was done to ensure that nothing had drifted.

D. Tune of the system for positive extraction

To search for positive FCP, the polarities of the target bias, extractor lens and 15° ESA power supplies had to be reversed. This ensured that all positive ions generated at the sputtering site were accelerated and transported to the charge exchange canal. As a preliminary to running the experiment, these ions were run through the cold canal and accelerated as positive ions to the LE cup. They, of course, could not be injected into

the accelerator. The beam current on the LE cup was $\sim 2nA$. The charge exchange canal heater was then turned on and the 70 kV accelerator and injector optics tuned for negative particles. Optimum transmission through the canal was obtained at a temperature of 175° C as read by the thermocouple, which sensed the external oven temperature. This resulted in $\sim 200pA$ of negative beam on the LE cup. One was now ready to inject beam into the accelerator.

The mass independence procedure was identical to that for the direct negative extraction case described in the previous section. Again there was an observable hydrogen beam which provided a means of fine-tuning the mass-independence. As the beam-related background is negligible in this search, the slits were taken completely out and did not impose any restriction on the beam trajectory.

The positive extraction search was run at $R = 1/3$ with 2MV on terminal. It had two independent stages of charge-state filtering. The first was provided by the charge exchange canal followed by the 30° cylindrical analyzer. The resolution of this analyzer was $\sim 4\%$ as calculated in section C of Appendix A. The second stage of filtering was the terminal stripper followed by the high energy analysis system. This system had a resolution of 0.2%. It is clear that the beam-related background for positive extraction is very much smaller than for direct negative extraction because of the extra stage of low-energy filtering. However, the total transmission will also decrease by about an order of magnitude, and so the resultant sensitivities actually turned out to be comparable.

It is necessary, for positive extraction, to scale the LE optics as well as the HE optics. For normal matter one has +1 ions leaving the sputtering site. These are accelerated through V_{ext}, charge exchanged to -1 in the charge exchange canal, and then accelerated through V_{table} to the LE cup. These particles then have

$$R_{integral} = \frac{1}{V_{ext} + V_{table}}.$$

Consider next FCP of charge $+1/3$ leaving the sputtering site. These are

accelerated through V_{ext}, charge exchanged to $-2/3$ in the charge exchange canal, and then accelerated through V_{table} to the LE cup. These particles have

$$R_{FCP} = \frac{2/3}{1/3\,V_{ext} + 2/3\,V_{table}}$$

$$\implies R_{FCP} = \frac{1}{1/2\,V_{ext} + V_{table}}.$$

One tuned the injection optics for integrally charged ions, and so for $R_{integral}$. The procedure, then, was to increase the table voltage by an amount equal to half the extraction voltage. This made R_{FCP} equal to $R_{integral}$ The LE optics was then tuned for FCP. The extractor bias was calibrated with a Fluke high voltage probe and dvm. This same high voltage measurement circuit was wired into part of the table voltage stack and the dvm output read with a TV monitor.

The $R = 1/3$ positive extraction procedure was then as follows. The mass independence was first setup, using the G.I. source. Then both the LE optics and HE optics were tuned for $R = 1/2$. The beam was put on the detector and the HE magnetic steerers and all degauss supplies on the system fine-tuned for optimum transmission of the hydrogen beam. Then the HE optics was scaled to the $R = 1/3$ background beam, i.e., $-1 \rightarrow +2 \rightarrow +1$. At this point the HE ESA voltages were fine-tuned to maximize the $R = 1/3$ background. Then the LE optics were scaled in the manner discussed in the preceding paragraph. The table bias was increased by an amount equal to half the target bias. Finally the HE ESA was scaled to the FCP setting. In doing this, one had to take into account the change in injection energy caused by the increase in table bias. One was now ready to take data.

Every hour during the search, the data acquisition was halted, and the above procedure iterated. This was done to ensure that there were no drifts in the system.

IV. Experimental Results

In this chapter the results of several searches for FCP in niobium and tungsten are reported. The niobium used in this experiment was 99.9% pure elemental niobium obtained from Alfa Products. The tungsten was in the form of a 15 mil thick sheet. Because it is a very hard substance, the tungsten was first heated, before machining with a diamond tool.

In section B, there is a discussion of how the sensitivity is calculated. It turns out that there are two different ways of analyzing the data, depending on whether one can measure the background or not. Sections C, D, and E describe the results for the respective searches $R = 1/3$, direct negative extraction, $R = 1/3$ positive extraction and $R = 2/3$, direct negative extraction.

A. Source output

(*i*) direct negative extraction

For direct negative extraction there was a steady beam current of ~ 2 nA on the low energy cup. However, when sputtering for the first time on a new target, beam currents as high as 20 nA could be extracted. This was generated by oxide layers on the surface and as the sputtering process cleaned the surface off, over a period of several hours, this current dropped to the 2 nA level. The targets were sputtered using magnetically analyzed argon in an ultra high vacuum environment and the naive expectation in the case of direct negative extraction was that the ions would be mainly the singly negative atomic ions of the target atom. However, on taking an $R = 1/2$ spectrum of the output, it was found from pulse height defect considerations that one obtained three peaks. This $R = 1/2$ spectrum is shown in Fig.11. One was certainly hydrogen as it gave a very narrow peak at 4 MeV. It was immediately obvious that this beam could be used to establish mass-independence at a mass of 938 GeV/c^2 and in addition to extend mass-independence down to 200 MeV/c^2.

There are two other peaks in Fig. 11. One is at around mass 20 and the other, the largest of the three, at about mass 35. The analyzing magnet was calibrated with known beams and then turned for these beams. It was found that the source output was $\sim$ 80% chlorine, $\sim$ 15% fluorine and $\sim$ 5% hydrogen.

One now had to determine the origin of the chlorine and fluorine. Clearly hydrogen is a major contaminant in all vacuum systems and so it was not that surprising that it showed up in the spectrum. The first thought was to analyze the residual gas in the vacuum system. All the vacuum components, as well as the copper target holders, were cleaned with solutions containing HCl. In addition, freon 113 with the chemical formula $C_2Cl_3F_3$ was used to cool the target holder and copper aperture. A leak from this system would give rise to the presence of chlorine and fluorine in the target chamber. Thus a residual gas analyzer (RGA) was attached to the target chamber. This demonstrated clearly that there were no chlorine or fluorine compounds in the residual gas of the system.

Another possibility was that some compound of chlorine or fluorine had a mass of 40 amu and so was a component of the sputtering beam. However, the extracted beam from the source was magnetically analyzed continuously between 0 and 50 amu and no chlorine or fluorine molecules were detected. Thus this possibility was ruled out.

The only possibility remaining was that the chlorine and fluorine were actually present in the sample. Thus a sample of the niobium was chemically analyzed and found to contain 2 parts per million of chlorine and not more than 0.1 parts per million of fluorine. If one assumes 100% ionization, extraction and collection of the chlorine atoms, then there is excellent agreement between the observed value of 2 nA of beam and the calculated value.

(ii) positive extraction

The direct positive extraction beam was initially accelerated posi-
tively charged to the LE cup. A beam current of 2 nA was measured.
Then, the charge-exchange canal heater was turned on, and the polarities
of the relevant power supplies reversed. A beam current of 200-300 pA of
negative beam was routinely obtained in this mode. Recalling that there
was a known transmission loss of 40-50% around the 30° esa, this would
imply a charge-exchange canal transmission efficiency of 20-30%.

This negative beam was then injected into the Pelletron, and an
$R = 1/2$ spectrum taken. This is shown in Fig. 12. Three peaks are indi-
cated. The peak at 4 MeV is clearly hydrogen, and this was used to estab-
lish mass-independence. Pulse height defect considerations were used to
determine the other two peaks. The higher energy peak, and larger of
the two, has a mass of 10-12 amu. The lower peak had a mass of $\sim$ 26
amu. There is an additional constraint. Because of the fact that they
charge-exchange in rubidium vapor with $\sim$ 20% transmission efficiency,
these particles must have high electron affinity. This would indicate that
the higher peak is probably carbon, and the lower peak silicon. Calcula-
tions of transmission efficiencies using the techniques of Appendix C
predict carbon to have a transmission efficiency of 15%, which is in rea-
sonable agreement with the observations.

B. Calculation of mass limits

Considerable effort was expended in this experiment to ensure that
the results be independent of FCP mass, over as large a mass range as
possible. This is necessary because the mass of an FCP is completely
unknown.

The lower mass limit is affected by two independent considerations.
Firstly, stray magnetic fields will place a lower limit on the mass. This
effect is biggest at the low energy end of the experiment where the ener-
gies of the particles are least. Hence they spend more time in the region
of stray fields and accordingly suffer greater displacements. The second

effect occurs in the high energy analysis system, where the high resolution of the system (.2%), means that relativistic effects enter.

Several precautions were taken to minimize stray magnetic fields in the extraction and injection regions. The target chamber, where the sputtered particles are first accelerated to ~ 8 keV energy, was enclosed in a bucking coil system. These coils bucked the earth's field in the horizontal and vertical directions normal to the direction of extracted beam. The resultant magnetic field in the chamber was measured with a Hall probe and found to be less than 0.05 gauss.

The injector was wrapped in high-permeability metal where possible, and the resulting magnetic field was found to be typically less than 0.1 gauss.

Consider a particle of mass m MeV/c^2, charge q (in units of e), and energy qV_{kV} keV travelling a distance l_{cm} cm through a region of constant magnetic field B_{gauss} gauss. Then the particle will obtain a perpendicular displacement Δx_{cm} cm, where

$$m = 4.5 \times \frac{10^{-5}}{V_{kV}}[B_{gauss}\frac{l_{cm}^2}{\Delta x_{cm}}]\frac{MeV}{c^2}.$$

This formula can be used to determine the lower mass limit if B is known. For

$$B = 0.1 \; gauss$$

$$l = 4 \, m$$

$$\Delta x = 1.25 \; cm$$

$$V = 78 \; kV$$

$$\implies m = 100 \; Mev/c^2.$$

The lower mass limit due to stray magnetic fields was conservatively taken to be 200 MeV/c^2.

The other constraint on the lower mass limit is fixed by relativistic effects in the HE analysis system. This system has a resolution of 0.2% and so relativistic effects are of consequence. These effects are discussed in detail in Appendix A. They constrain the lower mass limit to be around 200 MeV/c^2 and in the case of $R = 2/3$, $Z = 4/3$ particles, fix the lower mass limit at 250 MeV/c^2.

The upper mass limit is set by pulse height defect considerations. In general, the apparatus is capable of transmitting ions with masses of several hundred GeV/c^2. However, at high enough masses, the velocity of the incoming particle decreases sufficiently to lower the stripping cross-section significantly. The pulse height defect effects yield an upper mass limit much lower than this value. The pulse height defect of heavy atoms causes them to be progressively shifted toward the noise in the energy spectrum [cf. Fig. 14a]. Thus the lower extent of the FCP window was set at a pulse height defect value equal to that due to uranium ions. Hence, one quotes an upper mass limit of 240 GeV/c^2.

C. Discussion of estimated sensitivities

Here the estimated sensitivity obtained in the experiment is derived as a function of the measured parameters. It turns out that there are two methods of analyzing the data. The first takes all observed counts within the window to be FCP and obtains an upper bound on the concentration of FCP per target atom. The second assumes that one can measure the background in the window region and so subtract it. In what follows, 100% collection of secondary ions has been assumed. The system was designed to achieve this and there are two independent observations which lend support to this assumption. Firstly, the acceptance of the collection system was increased by a factor of two with no resulting increase in extracted beam. This was achieved by doubling the size of the extractor hole in the extraction plate. Secondly, the calculated value of extracted current based on 100% ionization and extraction of chlorine and fluorine is in excellent agreement with the observed value. Thus there is strong evidence for the assumption that there is 100% collection of the

secondary ions.

Another assumption involved in what follows is in relation to the transmission through the system of extracted beam from the argon source to the detector. The transmission was investigated carefully for beams with 2 MeV energy from the G.I. source. These transmission measurements are discussed in Chapter II, section D. Typically for everything heavier than oxygen, the transmission at 2 MeV was 5% from the L.E. cup to the FCP detector station. The transmission was then measured between the same cups for the FCP argon source and, for this beam, which was 80% chlorine, the number was 12%. In addition there was a 40% loss of beam in traversing the 30° ESA. Thus the low energy cup to FCP detector station transmission number was divided by a factor of two. A value of 6% for the transmission was then used for all particles heavier than helium for direct negative extraction.

Consider a beam of $I \mu$ A incident on the target. Let the sputter yield be S. Then the number of particles sputtered per unit time is

$$6.25 \times 10^{12} I S \quad \text{particles/second.}$$

Let the transmission from sputtering site to detector be t. Then the number of particles detected per unit time is

$$6.25 \times 10^{12} S I t \quad \text{particles/ second} \ .$$

Consider now a window in which FCP of a given electric rigidity and energy can be detected. Suppose there are N counts in T hours in a given search. Then we can analyze the data under two different assumptions

(i) no background measurement.

Here it is assumed that all of the N counts are FCP. Then there is an upper bound for the concentration per target atom, C, of

$$C = \frac{4.4 \times 10^{-17}}{S I t} \frac{N}{T}.$$

(ii) background measured.

Assume that B background counts are measured in one hour. Then in time T there will be BT background counts. In this time T there will have been detected

$$C = 2.25 \times 10^{16} \ S \ I \ t$$

FCP. Now if we demand an FCP signal 1σ above background we obtain

$$C = 6.28 \times 10^{-17} \ \sqrt{\frac{B}{T}} \frac{1}{S \ I \ t}.$$

One can see that in the case of a measured background the sensitivity goes as $T^{-\frac{1}{2}}$, whereas in the unknown case the upper bound goes as T^{-1}. The measured background case is relevant where the count rate is of the order or less than the beam-off background.

D. Results for R=1/3, direct negative extraction

The terminal potential during this run was 2 MV. The search was for $Z = N + 1/3$ N=1,2,.... particles, which came off the sputtering surface as a negative ion, i.e., had $EA \gtrsim 3.5eV$. The $Z = 1/3$ charge state was not in this group . It has an electron affinity of 1.5 eV, and so will come off positively charged.

Since one was looking for $Z = 4/3, 7/3,....$, a H_2 stripper was used. The detector employed was the thin ($20\mu m$ depletion depth), high field gradient Silicon surface barrier detector. This was located in the front cross of the detector station [cf. Fig. 8]. The FCP window in the energy spectrum was taken between 0.6 and 2.08 MeV. This covered all 2 MeV ions with masses up to 240 GeV/c^2. The 41.6 hours of data on the niobium target are shown in Fig. 13. The three peaks in this figure correspond to 6 MeV fluorine, chlorine and niobium, each with its distinctive pulse height defect. The FCP region is shown enlarged in Fig. 14a. Shown in Fig 14b is a spectrum of Rutherford scattered niobium with 2 MeV energy. An FCP with the mass of a niobium ion would yield this pulse height.

As indicated above, the main background in this search was from the 6 MeV $-1 \rightarrow +2 \rightarrow +1$ background scattering to lower energies. Several months of effort went into reducing this effect. The origin of this effect was in the pickup of an electron by the integer +2 charge state between the high energy end of the Pelletron accelerating column and the first set of plates in the high energy esa. Hence, one way of reducing the background was to improve the vacuum in this region, as the electron pickup probability is proportional to pressure. Before each run, the beamline in this region was baked for $\sim$ 36 hours with heating tapes. The pressure when running was $\sim 4 \times 10^{-7}$ torr. Once this background beam was formed, however, it had to scatter into lower energies. This came about by small angle scattering by the halo of the beam off the inside of the beampipe. A judicious choice of collimator sizes and positions reduced this effect.

As one can see from Fig. 14a, the niobium data look flat in the FCP region. However, the tungsten target produced a large tungsten component in the secondary beam. The probable cause for this is that the tungsten had a readily visible oxide layer on its surface. This layer was formed when the tungsten was heated in the machining process. Indeed, after several hours, the tungsten component in the beam had drastically decreased. This unexpected occurrence had two implications. Firstly, it indicated that the transmission of the system was good for heavy particles - tungsten has a mass of 184 amu. On the other hand, however, it produced a much bigger background in the FCP region. This was because the 6 MeV tungsten peak was pulse height defected to $\sim$ 3 MeV. Hence, there was a large scattering tail into the FCP window region. As a result, the running time for the tungsten target was only 7.4 hours, whereas the niobium was sputtered for 41.6 hours.

The total numbers of counts in the FCP region for $R = 1/3$ direct negative extraction are given in Table 1. The transmission from sputtering site to detector was taken to be 6%. The sputtering yield for 30 keV Ar^+ on niobium was measured to be 6.3, in good agreement with the calculated value. The sputtering yield for tungsten was taken to be 2.5.

Assuming 27 μA of Ar$^+$ sputtering beam, one calculates an upper bound for the integral (i.e., a sum over all species of FCP) FCP concentration to be 2.8×10^{-17} per atom and 4×10^{-16} per atom for niobium and tungsten, respectively. If one does a peak search for one species of FCP, one obtains 1.5×10^{-18} /atom and 1×10^{-16} /atom, respectively.

E. Results for R = 1/3 , positive extraction

Here one was covering those sections of the $Z = N + 1/3$ table not covered in the $R = 1/3$ direct negative extraction search; i.e., fractionally charged atoms with $EA \lesssim 3.5\,eV$. A $Z = N + 1/3$ FCA cannot come off neutral (except possibly as a molecule of FCA s), and so must come off either positive or negative. By doing both positive and negative extraction, all possibilities have been covered, even though we cannot predict with certainty whether a given FCP will come off positive or negative. Because the particles came off the sputter target positive, it is necessary to charge-exchange them in the rubidium charge-exchange canal before injection. As discussed in Chapter III, section D, when the system was tuned for FCP there was zero beam current impinging on the detector.

There were two distinct experiments to be done for each of the niobium and tungsten targets. There was a run with the N_2 stripper, which was most sensitive to $Z = 1/3$ particles. This used the gas ΔE, Si1, and Si2 detectors at the rear of the detector station, as shown in Fig. 8. Secondly, there was a run with the H_2 stripper, which looked for heavy ions; i.e., $Z = N + 1/3$;N = 1,2,...; $1\,GeV/c^2 \lesssim m \lesssim 240\,Gev/c^2$. These two experiments will be discussed separately.

(i) $Z = 1/3$

The terminal potential was 2 MV for this run. One used the N_2 stripper as one was searching for lightly ionizing particles. The gas ΔE-Si1-Si2 detector system was used, with the trigger on Si1 set at below 250 keV. For each event Gas, Si1, Si2, Gas vs. Gas+Si1, and Si2 vs. Si1+Si2 were recorded. Of course, because of the low-energy charge filter, there

was essentially zero beam-generated events recorded here. The main source of background was due to cosmic ray generated events in Si1 [cf. Fig. 9]. The detector system was shielded as effectively as the geometry would allow by four plastic scintillator paddles. The output of these paddles was used to veto the cosmic ray events cf. Fig. 10. The HE slits were fully open for this run.

28 hours of data were taken on the niobium target and 17 hours on the tungsten.

The window for FCP in this run is not so obvious as for the direct extraction case. Consider a 2.05 MeV fractionally charged particle incident on the detector. Its electronic stopping power will be described by the Bethe-Bloch formula, and so we may scale from the stopping power of a proton of the same energy

$$\left[\frac{dE}{dx}\right]_{Z=\frac{1}{3}} = \frac{m}{9}\left[\frac{dE}{dx}\right]_H.$$

Si1 has a thickness of 116 mgcm^{-2} of silicon. The thickness of Si2 is 14 mgcm^{-2}. If one scales the range, one finds that all $Z = 1/3$ FCP s with masses greater than 0.9 GeV/c^2 will stop in Si1. Clearly, as the mass of the FCP decreases, it will leave less energy in Si1. The lower mass limit is 0.2 GeV/c^2 and this particle will leave ~ 0.3 MeV in Si1. Thus a window in Si1 from 0.3 to 2.05 MeV will include all $Z = 1/3$ particles with mass greater than 0.2 GeV/c^2.

A 24-hour background run was taken with the beam off. With allowance made for the different running times, the background spectrum was subtracted from the data spectrum. This difference was then scanned in bins of 100 keV width to search for a peak. 100 keV was the estimated 3σ width of a peak. σ was obtained by adding in quadrature the straggling broadening and the detector resolution. The bin center was directly related to the mass of a $Z = 1/3$ particle by calculating the energy lost in Si1 as a function of mass. The concentration for each bin center was calculated as follows. For a given bin center, the larger of the

beam-on beam-off difference and the statistical error was taken as the effective number of counts in that bin. The transmission from LE cup to FCP cup was taken to be 50%. The transmission from the sputtering site to the LE cup was determined as a function of mass using the procedure outlined in Appendix C. The Ar^+ sputtering beam current was assumed to be 27 μA. The sputtering yields for niobium and tungsten were taken as 6.3 and 2.5 respectively. The result was a plot of concentration per target atom vs. FCP mass. These plots are shown for niobium and tungsten respectively in Fig. 15 and Fig. 16. The integral concentration was calculated to be 1×10^{-17} and 2.5×10^{-17} respectively for niobium and tungsten. The transmission from the sputtering site to the LE cup was taken to be 10% in this calculation.

(ii) $Z = N + 1/3$; N=1,2,... , $EA \lesssim 3.5\,eV$

The terminal potential was 2 MV for this search. Because we were looking for heavily ionizing particles, the H_2 stripper was used. For this reason also, the thin, high field gradient silicon detector at the front of the detector station was used. The threshold was set below 250 keV. Again, because of the low-energy charge filter, there were no beam generated events here. The main source of background events was room γ-rays. Thus, the detector was shielded with $\sim 2''$ of lead. 40 hours of data were taken on the niobium target and 24 hours on the tungsten. The FCP energy window for this search was identical to that for the $Z = N + 1/3$ direct negative extraction search, i.e., 0.65 to 2.05 MeV.

A 48-hour background run was taken with the beam off. With allowance made for the different running times, the background spectrum was subtracted from the data spectrum. The resulting spectrum is shown in Fig. 17. This spectrum was then scanned in bins of 150 keV width to search for a peak. This was the estimated 3σ width of a peak. The bin center was directly related to the mass of a $Z = N + 1/3$ FCP by pulse height defect considerations [cf. Appendix B]. The concentration upper limit for each bin center was then calculated. The larger of the beam-on, beam-off difference and the statistical error was taken as the

effective number of counts in that bin. The transmission from LE cup to FCP cup was taken to be 6%. The transmission from the sputtering site to the LE cup was determined using the procedure outlined in Appendix C. In general, this number depended on mass. However, the lowest transmission value of 10% was conservatively taken. This corresponds to an electron affinity of 0.8 eV. The Ar^+ sputtering beam current was taken as 27 μA. The result was a plot of upper limit concentration per target atom vs. FCP mass. These plots are shown for niobium and tungsten, respectively, in Fig. 18 and Fig. 19.

F. Results for R = 2/3 ,direct negative extraction

Here we search for $Z = N + 2/3$; N=0,1,2.. particles. Also one is sensitive to $Z = 4/3$ *via* $-2/3 \rightarrow +4/3$ charge exchange, i.e., the stripping of two electrons. Unfortunately, $R = 2/3$ is the rigidity of the $-1 \rightarrow +2$ integral charge state. Thus, if one tunes for $R = 2/3$, there is in general a beam current of hundreds of picoamperes on the FCP detector cup. It had been hoped that it might still be possible to attempt a search for these $Z = N + 2/3$ particles by looking at two electron ($R = 5/6$) or three electron ($R = 8/9$) strippings at the terminal. However, in the former case the background was again too large, whereas, in the latter, the scaling to such a high charge state was not reliable.

Hence, the strategy adopted was to place a 3.4 $mgcm^{-2}$ aluminum foil on the window of the gas detector to stop all integrally charged ions heavier than lithium. It was then possible to look for $Z = 2/3$, $4/3$, and $5/3$ FCP.

The terminal potential on the Pelletron during this run was 3 MV. This was necessary to give higher mass FCP a sufficient range to reach the detector.

There were some interesting observations made during this run. Consider an H_2^- ion incident on the terminal stripper. With very high probability it will break up, generating at least one H^+ a large fraction of the time. At the high energy analysis system these H^+ will have energy 1.5

eV_T , where V_T is the terminal potential. Thus a peak at 4.5 MeV was observed in the Si1 energy spectrum. Indeed, another peak at 9 MeV was also seen, which corresponded to the simultaneous detection of the two 4.5 MeV protons from the same incident H_2^- molecule.

There was a curious peak which left 0.32 MeV in the gas detector and a total energy of 1.2 MeV in Gas+Si1. The rate in the peak was measured as a function both of stripper thickness and target material as follows;

target	stripper gas	stripper pressure	rate $\overline{hr^{-1}}$
W	H_2	800μm	147
W	N_2	800μm	296
Nb	H_2	800μm	995
Nb	N_2	800μm	709
Nb	N_2	100μm	2890

Decreasing the stripper thickness resulted in a large increase in rate. This observation supports a molecular interpretation. Using Bethe-Bloch energy loss, one obtains that a 1.2 MeV deuteron would lose 0.34 MeV in the gas detector. This implies that the best candidate is a 1.9 MeV deuteron losing 0.7 MeV in the 3.4 $mgcm^{-2}$ window. This deuteron was accelerated to the terminal while bound in a molecule.

The detector used was the Gas ΔE-Si1-Si2 system, triggered at ~ 250 keV on Si1. For each event, Gas, Si1, Si2, Gas vs. Gas+Si1, and Si2 vs. Si1+Si2 were recorded.

Because of their 2 electron change at the terminal, the $Z = 4/3$ particles will have 6 MeV. The $Z = 2/3, 5/3$ particles will have 3 MeV. The data analysis divides accordingly.

(i) $Z = 4/3$

Here we look for 6 MeV $Z = 4/3$ particles. The N_2 stripper was used, as two electrons were being stripped.

We demand that a $Z = 4/3$ particle make it into the Si1 detector. This puts an upper mass limit of 14 GeV/c^2 on the mass of such a particle. Consideration of relativistic effects at the high energy analysis system [cf. Appendix A], puts a lower mass limit of 0.3 GeV/c^2.

The data were analyzed using the Gas vs. Gas+Si1 spectrum. This is a two-dimensional 128×128 spectrum, called DEE, with a gain of 80 keV per channel. Three cuts were placed on the data. Firstly, all counts with Gas+Si1 > 6.05 MeV were rejected. Secondly it was demanded that the energy lost in the 0.77 mgcm^{-2} Gas detector be large enough to be not completely inconsistent with the energy lost by the particle in the 3.4 mgcm^{-2} aluminum window. Finally, it was demanded that the particle deposit at least 240 keV in Si1.

After these cuts were made, there remained for the 2-hour run on niobium, 45 counts in the window. 44 of these counts were in a peak at 3.09 MeV in the Gas, and at 3.65 MeV in Gas+Si1. By energy loss considerations, these could not be FCP. They were identified as 9 MeV lithium ions. A 9 MeV lithium ion would lose ~5.5 MeV in passing through the aluminum window, in agreement with the observation. There remained 1 count. This left 0.16 MeV energy in the Gas detector and 5.57 MeV in Gas+Si1. This was a $Z = 4/3$ FCP candidate with a mass of 1.6 ± 0.5GeV/c^2. It gave a limit of 5.2×10^{-19} for both the peak and integral concentrations for niobium.

A similar analysis was applied to the 2-hour run on tungsten. After the above cuts were made, there remained 41 candidates in the window. 33 of these were in a peak at 2.53 MeV in the Gas detector and 3.17 MeV in Gas+Si1. It is to be noted that the starting energy of these particles is ~0.5 MeV lower than in the niobium spectrum. This could be explained by inhomogeneities in the aluminum window. It is likely that these particles observed are the straggling tail of a huge peak. From energy

considerations, these 33 events could not be FCP. 2 other events could similarly be eliminated. There remained the following six candidates.

COUNTS	$\dfrac{\text{Gas}}{\text{MeV}}$	$\dfrac{\text{Gas+Si1}}{\text{MeV}}$	$\dfrac{\text{Mass}}{\text{GeV}/c^2}$
1	1.9±0.04	3.0±0.04	10±1
1	0.5±0.04	4.8±0.04	4.2±0.5
3	0.2±0.08	5.4±0.08	2.1±0.5
1	0.1±0.04	6.0±0.04	0.2±0.1

The errors quoted are purely statistical. There is an added systematic error because of uncertainty in the energy loss tables of the order of 20%.

This gives integral and peak limits of 7.8×10^{-18} and 5.9×10^{-18}, respectively, for tungsten.

Consider these 7 candidate events for a fractionally charged particle. It is possible to understand these events using integrally charged particles. Consider the peak of three events in the tungsten run and the single event in the niobium run. These four events are thought to be due to 5.486 MeV α-particles on the surface of the silicon detector detected in coincidence with noise in the gas detector. A 24-hour background run was taken with the beam off and 8 counts were obtained in a peak at 0.14 MeV in the Gas and 5.4 MeV in Gas+Si1. All silicon detectors used in this experiment indicated contamination with Am^{241} when background runs of the order of days were taken. It is presumed that this contamination originates in the energy resolution measurement at the factory.

The other events are less easy to explain. One can identify the 10 GeV/c^2 candidate as a 3 MeV α-particle which will lose ~1.7 MeV in the gas detector, in agreement with the observation. One can explain the 4.2 GeV/c^2 event by identifying it as a 4.8 MeV He^3. Likewise, a 6 MeV deuteron will leave ~0.12 MeV in the gas detector. However, it is difficult to

come up with a plausible explanation of how one obtains a 3 MeV α-particle, a 4.8 MeV He^3 atom , and a 6 MeV deuteron inside the gas detector. Clearly, what are needed are more measurements. It should be possible by running longer, moving about in rigidity space, and varying the gas detector pressure to obtain a better understanding of these events.

(ii) $Z = 2/3$

Here we searched for 3 MeV $Z = 2/3$ particles in the DEE spectrum. The N_2 stripper was used.

We demand that a $Z = 2/3$ particle make it into, and trigger the Si1 detector. This puts an upper mass limit of 15 GeV/c^2. A lower mass limit of 0.2 GeV/c^2 is set by stray magnetic fields.

The data were analyzed using the DEE spectrum as before. Four cuts were put on the data. Firstly, all counts with Gas+Si1 > 3.025 MeV were rejected. Then it was demanded that the energy lost in the gas detector be large enough to be not completely inconsistent with the energy lost in the 3.4 mgcm^{-2} aluminum window. Thirdly, it was demanded that the particle deposit at least 240 keV in Si1. Finally, all particles with energy less than 240 keV were rejected. This was possible because the maximum energy lost by a 3 MeV $Z = 2/3$ particle in 3.4 mgcm^{-2} of aluminum was determined to be 1.7 MeV.

After these cuts were made, there remained 206 events in the 2 hour run on niobium. This resulted in an integral concentration upper limit of 1.3×10^{-16}. A peak search was then made in the data using a 4 σ wide bin of 80 keV. This resulted in a peak concentration limit of 2.2×10^{-17}.

For the 2-hour run on the tungsten target, there remained 532 counts after the above cuts were made. This resulted in integral and peak upper limits of 6.9×10^{-16} and 1.2×10^{-16}, respectively.

(iii) $Z = 5/3$

Here we search for 3 MeV $Z = 5/3$ particles. As Z is now higher, an H_2 stripper was used. Thus the transmission used was 6%.

We demand that a $Z = 5/3$ particle trigger in Si1, so we obtain an upper mass limit of 4 GeV/c^2. A lower mass limit is obtained from stray magnetic fields of 0.2 GeV/c^2.

The data were again analyzed using the DEE spectrum. Three cuts were put on the data. All events above 3.025 MeV were rejected. It was demanded that a particle leave 240 keV in Si1. Finally, the low Gas events which could not be FCP were eliminated.

After these cuts were made, there remained 7 counts in the 6-hour run on niobium. These were in the tail of a distribution originating outside the FCP window and so were not FCP candidates. They fixed the FCP concentration upper limit at 4.9×10^{-18}.

After the above cuts were made to the data on the 6-hour run on tungsten, there remained 8 counts. These again were due to a background tail. They fixed the $Z = 5/3$ FCP concentration limit in tungsten at 1.3×10^{-17}.

G. Conclusions

We have searched in samples of niobium and tungsten for $Z = N + 1/3$; N=0,1,2,... and $Z = N + 2/3$ N=0,1 for evidence of modulo 1/3 fractionally charged particles. Upper limits for the FCP concentrations per target atom were measured. The limits obtained in these measurements are summarized in Table 1, Table 2, and Figures 15,16,18, and 19. Table 1 with Figures 15 and 18 gives a summary of the data on niobium. The tungsten results are summarized in Table 2 and Figures 16 and 19. We recall from Chapter I that, if there were one FCP on a typical sphere in the Stanford experiment, then this would imply a concentration per atom of 1.7×10^{-18}. One can see that many of the upper limits reported here are lower than this number. Thus under the assumptions of this experiment, the data set severe constraints on the types of

fractional charge that the Stanford group can be observing. In the case of niobium, all $Z = 1/3$ particles with a mass between 0.5 and 250 GeV/c^2, all $Z = 4/3$ particles with a mass between 0.3 and 14 GeV/c^2, and all $Z = N + 1/3$ particles with a mass between 0.5 and 240 GeV/c^2 are measured to have concentration upper limits equal to or less than the observed FCP concentration at Stanford. The best limit obtained was for $Z = 4/3$ particles , where some interesting events were observed. This case clearly warrants further study. It is of particular interest because of the prediction of Slansky, Goldman, and Shaw in 1981. They predicted that the symmetry-breaking of QCD could lead to the existence of free, low-mass, fractionally charged diquark states.

The results completely negate the arguments of Morgan and Barnhill 1983, who predicted FCP concentrations in tungsten of 10^{13} to 10^{14} per tungsten atom on the basis of statistical arguments. The direct negative extraction limits for tungsten are about a factor of fifty larger than for niobium. This was due to the large tungsten component in the secondary beam caused by the oxide layer created on the tungsten surface during the machining process.

Consider now how one might improve on these limits. All concentration limits reported depend inversely on the primary sputtering beam and linearly on the background rate per unit time. It might be possible to increase the primary argon beam current from its present 30 μA to 100 μA. This would give a corresponding improvement in the limits, if the background rate is independent of beam. As regards the background rate reduction, it is hard to see one doing much better in the $R = 1/3$ case. The direct negative extraction measurements are limited by the $-1 \rightarrow +2 \rightarrow +1$ background. It is unlikely one can do much better with the present apparatus. One possibility is to add a further stage of electrostatic analysis. This would certainly result in a decrease in background rate. However, the range of mass over which the system would be mass independent would decrease substantially because of the relativistic considerations in Appendix A. In the case of $R = 1/3$ positive extraction, the background is determined by cosmic-ray generated events in Si1. In

this case, a larger sputtering beam will clearly help. For the lower mass region of this search, one is limited by counting statistics, so running for longer times will clearly help here.

The $R = 2/3$ case will certainly profit from longer running times. In particular, in the $Z = 4/3$ search it should be possible to improve the present limits by an order of magnitude. One possibility of decreasing the background for this search might be to place the 3.4 mgcm^{-2} aluminum foil just after the analyzer plates. This would enable much of the incident beam to multiply scatter, and so it would not reach the detector.

APPENDIX A

The Theory of Electrostatic Systems

In this appendix, the behavior of charged particles in purely electrostatic fields is discussed. This discussion is important because the experiment was designed to be mass-independent as far as possible. This was necessary because the mass of an FCP is completely unknown. Recall that for magnetic fields the applied force depends on the mass of the particle. In purely electrostatic fields, however, as we shall see, the trajectory of the particle is independent of its mass.

A. Non-relativistic trajectories

In this section, the behavior of non-relativistic charged particles in electrostatic fields is discussed. This is important because, apart from relativistic effects due to the very high resolution of the high-energy electrostatic analysis system, it describes the trajectories of particles through the experimental apparatus.

Consider a charged particle of mass m, charge q, kinetic energy T and velocity $\mathbf{v}$ moving in an electrostatic field described by the potential $\varphi(\mathbf{r})$. Then this system has a Lagrangian

$$L = \frac{1}{2}m\mathbf{v}^2 - q\,\varphi(\mathbf{r}).$$

The trajectory of the particle between times t_1 and t_2 is specified uniquely by the condition that

$$\int_{t_1}^{t_2} L(\mathbf{r},\mathbf{v},t)\,dt$$

takes the least possible value. This, of course, is the principle of least action. Clearly, multiplication of the Lagrangian by a constant factor does not change the equations of motion. If L is multiplied by $1/q$, the following equivalent new Lagrangian, L', is obtained

$$L' = \frac{T}{q} - \varphi(\mathbf{r}).$$

It is clear that all particles with the same initial value of

$$\frac{T}{q}$$

whose trajectories coincide at t_1 will describe the same trajectory to t_2, if their charges do not change. This quantity, T/q, is called the electric rigidity of the particle. It is easy to see why it is called this. The larger the kinetic energy, or the smaller the charge, the less effect the electric field will have on the particle's motion, and hence the more rigid it will be. It is analogous to the quantity

$$\frac{p}{q}$$

for a magnetostatic field. Indeed, this may also be shown by means of a similar argument if a term

$$q \ \mathbf{v}.\mathbf{A}(\mathbf{r})$$

is added to the Lagrangian. Here $\mathbf{A}(\mathbf{r})$ is the magnetic vector potential.

The quantity used throughout the text of the thesis is inversely proportional to the electric rigidity and is denoted by R; i.e.,

$$R = \frac{q}{T} V_T$$

where V_T is the Pelletron terminal potential.

Consider the statement of conservation of energy. Let any particle start from rest ,at the origin, in an electrostatic field. Take the zero of potential to be at the origin. Then

$$T(t) = -q \ \varphi(\mathbf{r})$$

$$\implies \frac{T(t)}{q} = -\varphi(\mathbf{r}).$$

Thus all particles, independent of their mass, have the same value of

T/q if they all start from rest at the same point. However, it has just been demonstrated that all particles with the same initial trajectory and value of T/q describe the same further trajectory in an electrostatic field, if their charges do not change. The following theorem is then proved.

Theorem

In the non-relativistic approximation, the trajectories of all particles starting from rest at a given point in an electrostatic field are independent of the particles' charges and masses.

This theorem is basic to the understanding of the sputter source. Thus the extraction and injection optics are all purely electrostatic, and so all charged particles which start from rest at the sputtering site will follow the same trajectory independent of both mass and charge.

The realization that the electric rigidity defines the trajectory of a charged particle in a purely electrostatic field gives insight into how the charge changing process acts as a filter in this experiment. What happens in a charge changing process, e.g., at the charge exchange canal on the injector or at the stripper canal in the pelletron terminal, is that the electric rigidity is changed by a large amount, typically 50-100%. If this charge-exchange is followed by an electrostatic analysis system with ~1% resolution, then it is clear that a large rejection of background can be achieved. Indeed, this is what is done in the experiment. The injector charge-exchange canal is followed by a 30° cylindrical electrostatic analyzer with ~2% resolution. The high energy analysis system has a resolution of ~0.2%.

B. Relativistic motion of charged particles in a uniform electric field

Consider a fast-moving charged particle incident on a parallel plate ESA. Let the particle have mass m, charge q, and velocity v. Define, in the usual notation,

$$\beta = v/c.$$

Let the plates have length L, gap d, and potential V between them. The equation of motion of the particles is given by the relativistic Lorentz force equation

$$\frac{dP^\mu}{d\tau} = qF^{\mu\nu}U_\nu$$

where $P^\nu = mU^\mu$ is the 4-momentum; $u_\nu = (\gamma, \gamma\mathbf{u})$ is the 4-velocity and $F^{\mu\nu}$ is the electromagnetic field tensor. It is straightforward to solve this equation for the given problem. When this is done, an expression is obtained for the angle θ between the incoming direction of the particle and its outgoing direction

$$\tan\theta_{elec} = \frac{1}{\beta}\sinh\left[\frac{qV}{m}c^2\frac{L}{d}\frac{1}{\beta\gamma}\right].$$

Now for the situation under consideration the argument of the sinh function is small so we may use the approximation

$$\sinh x = x + \cdots$$

for small x. Then taking the non-relativistic limit $\gamma \to 1$ we obtain

$$\tan\theta = \frac{L}{d}\cdot\frac{V}{2}\left[\frac{q}{\frac{1}{2}mv^2}\right]$$

which is exactly the expression used in the non-relativistic regime. The electric rigidity is then the relevant parameter to use. However, we see that in the exact relativistic expression no such quantity appears and so in general the trajectory is different for particles of different charge and mass. Thus, the question is raised of how particles of different masses between 200 MeV/c^2 and 200 GeV/c^2 would behave in the analysis system. It is clear that relativistic effects will become more important as the mass of the particle decreases or as its energy rises. Hence it is important to know, for example, where a 200 MeV/c^2 FCP with charge +1/3 will end up, having passed through the high energy analysis system.

Consider the $R = 1/3$ experiment with 2 MV on terminal. Recall that the analysis system is initially tuned with $R = 1/2$ niobium. This is achieved with 50 kV across the plates. The effective length of the plates is 90 cm and the gap between them is 3 cm. For a 4 MeV singly charged niobium ion

$$\beta = 9.58 \times 10^{-3}$$

$$\gamma = 1.00046$$

and the bend angle is $10.6097°$.

The drift region after the plates is 6m long, so the effective displacement is 1123.9 mm. The mass-independence procedure used in the experiment then entailed sending a proton beam through this system and adjusting a small magnetic field approximately 6m before the electrostatic system so that the protons ended up in exactly the same position as the niobium beam at the detector station. If one considers the motion of a charged particle through a uniform $\mathbf{B}$ field normal to the initial direction of motion of the particle, one obtains a similar expression to the electric case except that the qv/d is replaced by $q\beta B$. Thus

$$\tan\theta_{mag} = \frac{1}{\beta}\sinh\left[\frac{qBL}{mc}\cdot\frac{q}{\gamma}\right].$$

If the protons are to end up with the same net displacement as the niobium ions, then

$$1123.9\text{mm} = 6000\left[\tan\theta_{elec} - 2\tan\theta_{mag}\right]$$

where the angles on the right-hand side are for the proton. A 4 MeV proton has

$$\beta = 9.21 \times 10^{-2}$$

$$\gamma = 1.00426.$$

This implies $BL = 8.55375 \times 10^{-5}$ Tm .

One now proceeds to go to $R = 1/3$ and tunes the system so that a 2 MeV niobium FCP with $q = +1/3$ has a displacement of 1123.9mm. BL remains fixed at its value determined at $R = 1/2$. A 2 MeV niobium ion has

$$\beta = 6.766 \times 10^{-3}$$

$$\gamma = 1.000023.$$

The potential at $R = 1/3$ is the 74.814 kV. A 2 MeV proton will be displaced 2.2 mm away from the niobium position, on the side of decreasing θ. However, a particle with mass 200 MeV/c^2 and energy 2 MeV will be displaced 0.4 mm from the niobium position on the side of increasing θ. Thus all particles with masses greater than 200 MeV/c^2 will fall within a 2.6 mm wide band. The actual slit used had a width of 6mm so clearly one can state with confidence that all particles with masses greater than 200 MeV/c^2 were transmitted through the analysis system to the detector station.

Next consider the case of $R = 2/3$ with 3 MV on terminal. To establish mass independence at $R = 1/2$, the requirements are

$$V = 74.9353\text{kV}$$

$$BL = 1.12379 \times 10^{-4}\text{Tm}.$$

At $R = 2/3$ this implies

$$V = 56.1208kV.$$

The protons and 200 MeV/c^2 mass particles are displaced, respectively, 3.2mm and 0.7 mm from the niobium position, both on the side of decreasing θ. Thus all particles with a mass greater than 200 MeV/c^2 fall in a band of width 3.2 mm.

C. Electrostatic analyzer resolution

Loosely defined, the energy resolution of an analyzer is the fractional bite in energy which the analyzer samples. Clearly the lower this number is, the more rejection in background can be obtained. This section is divided into two parts. First, the case of a cylindrical analyzer is discussed. This was the case of the 15° and 30° ESAs on the injector. Then, because the analysis is a little different, the case of a parallel plate analyzer is considered. This was the geometry used in the analysis system at the high energy end of the machine.

(i) Cylindrical ESA

Let us consider a cylindrical analyzer of central radius ρ, gap d, and length l. Take x to be the direction in the bending plane perpendicular to the central ray and y normal to the bending plane. Let x' and y' be the slopes of the rays in the x- and y- directions. Let δ be the fractional energy spread in the beam, i.e.,

$$\delta = \frac{\Delta E}{E} \ll 1.$$

The quantities (x_2, x'_2, δ) and (y_2, y'_2) after the analyzer are related to their values (x_1, x'_1, δ) and (y_1, y'_1) before the analyzer by

$$\begin{pmatrix} x_2 \\ x'_2 \\ \delta \end{pmatrix} = \begin{pmatrix} \cos\sqrt{2}\theta & \frac{\rho}{\sqrt{2}}\sin\sqrt{2}\theta & \frac{\rho}{2}[1 - \cos\sqrt{2}\theta] \\ -\frac{\sqrt{2}}{\rho}\sin\sqrt{2}\theta & \cos\sqrt{2}\theta & \frac{1}{\sqrt{2}}\sin\sqrt{2}\theta \\ 0 & 0 & 0 \end{pmatrix} \begin{pmatrix} x_1 \\ x'_1 \\ \delta \end{pmatrix}$$

$$\begin{pmatrix} y_2 \\ y'_2 \end{pmatrix} = \begin{pmatrix} 1 & \rho \\ 0 & 1 \end{pmatrix} \begin{pmatrix} y_1 \\ y'_1 \end{pmatrix} .$$

The matrices which relate values before and after the analyzer are called transfer matrices. If we have drifts of lengths L_1 and L_2 on the entrance and exit sides, respectively, then the horizontal transfer matrix becomes

$$\begin{bmatrix} 1 & L_2 & 0 \\ 0 & 1 & 0 \\ 0 & 0 & 1 \end{bmatrix} \begin{bmatrix} \cos\sqrt{2}\theta & \frac{\rho}{\sqrt{2}}\sin\sqrt{2}\theta & \frac{\rho}{2}[1-\cos\sqrt{2}\theta] \\ -\frac{\sqrt{2}}{\rho}\sin\sqrt{2}\theta & \cos\sqrt{2}\theta & \frac{1}{\sqrt{2}}\sin\sqrt{2}\theta \\ 0 & 0 & 0 \end{bmatrix} \begin{bmatrix} 1 & L_1 & 0 \\ 0 & 1 & 0 \\ 0 & 0 & 1 \end{bmatrix}.$$

Energy resolution of this system is defined as follows. The energy resolution is defined as the maximum value of δ which the beam can have entering the system and still be transmitted through it entirely. Clearly the resolution depends on the lengths of the drifts before and after the analyzer and also the slit dimensions. Using the above horizontal transfer matrix one obtains

$$x_2 = \left[\cos\sqrt{2}\theta - \sqrt{2}\frac{L_2}{\rho}\sin\sqrt{2}\theta\right]x_1 + \left[L_1\cos\sqrt{2}\theta + \frac{\rho}{\sqrt{2}}\sin\sqrt{2}\theta\right]\delta.$$

Let us evaluate the resolution for the case of the 30° ESA on the injector. Here we have a 1″ aperture 15cm in front of the analyzer and another 1″ aperture 100 cm downstream of the aperture. Thus with

$$L_1 = 15\text{ cm} \quad , \quad L_2 = 100\text{ cm}$$

$$x_2 = x_1 = 1.25\text{ cm}$$

$$\rho = 122\text{ cm} \quad , \quad \theta = 30°$$

we have

$$\delta = 2\%.$$

An important assumption in this analysis is that there are no fringing effects at the entrance and exit to the plates. In practice what one does is to place field clamps at the entrance and exit. These are grounding plates which are placed close to the plates and pull the field lines parallel to the surfaces of the plates. In this way, one does not have significant focussing effects due to fringing fields. This focussing effect increases with the ratio of plate voltage to beam energy. Thus it was found important to include field clamps for the 15° and 30° cylindrical analyzers at

the low energy end where

$$\frac{V}{E} \approx \frac{10}{70}.$$

However, it was not important at the high energy end where

$$\frac{V}{E} \approx \frac{24}{2000}.$$

In addition, it was found important to balance the voltage on the analyzer, i.e., run one plate at $+\dfrac{V}{2}$ and the other at $-\dfrac{V}{2}$. If the beam is broad, i.e., of the order of the analyzer gap width, then if one plate is grounded and the other is at $+V$, there will be a significantly different focussing effect on each side of the plate. The voltage was balanced for all analyzer systems in this experiment.

Another consideration is the effective length of the plate. Because of fringing effects, the actual length is shorter than the effective length. This effective length was calculated for the high resolution high energy analysis system using the Herrmannsfeldt program. For the case of plates with field clamps, the effective length can be determined analytically [cf. Wollnick 1965].

(ii) parallel plate ESA

Consider here a system of parallel plates of length l, gap d, and with voltages $\dfrac{+V}{2}$ and $\dfrac{-V}{2}$. Let a particle of mass m, charge q, and energy E be incident parallel to the plates. Then the transverse distance y moved by the particle after transversing the plates is

$$y = \frac{1}{4} \frac{qV}{E} \frac{l^2}{d}.$$

Also the angle the direction of motion of the particle makes with the incident direction after transversing the plates is

$$\tan \theta = \frac{1}{2} \frac{qV}{E} \frac{l}{d}.$$

If the analyzer system is followed by a drift section of length L and a slit of width w, then clearly

$$\delta = \frac{\Delta E}{E} = \frac{w/2}{\frac{qV}{2E}\frac{l}{d}[L + \frac{l}{2}]}.$$

Let us evaluate the resolution for the case of the first section of the high energy analysis system. Here

$$V = 25 \text{ kV} \qquad E = 4000 \text{ kV}$$

$$l = 30 \text{ cm} \qquad d = 3 \text{ cm}$$

$$W = 0.5 \text{ cm} \qquad L = 600 \text{ cm}.$$

This gives

$$\delta = 1.35\%.$$

D. Scaling between different charge states

Here the scale factor used in scaling from one charge state to another is derived. As shown above, the trajectory of a charged particle in a system of electrostatic fields is a function only of R where

$$R = \frac{q}{E} V_T.$$

Consider first the case of direct negative extraction. Thus for a particle which is extracted with a charge $-q_1$, injected into the pelletron with injection $q_1 V_{INJ}$, accelerated to a terminal potential V_T, stripped to a charge state $+q_2$, and then electrostatically analyzed, we have

$$R = \frac{q_2 V_T}{(q_1 + q_2)V_T + q_1 V_{INJ}}.$$

Typically $V_{INJ} = 78 \text{ kv}$, $V_T = 2 \text{ MV}$ so

$$\frac{V_{INJ}}{V_T} = .039$$

and

$$R = \frac{q_2}{q_1 \, 1.039 + q_2}$$

for direct negative extraction.

For positive extraction we first accelerate $+q_0$ to V_{ext}, charge exchange to $-q_1$, accelerate to $q_0 V_{ext} + q_1 V_{table}$, then inject as $-q_1$, accelerate to a terminal potential of V_T, strip to $+q_2$ and then analyze. One then has

$$R = \frac{q_2}{q_2 + q_1[1 + \dfrac{V_{table}}{V_T}] + q_0 \dfrac{V_{ext}}{V_T}}.$$

Typically $V_{table} = 70\text{kV}$, $V_{ext} = 8\text{kV}$, $V_T = 2000\text{kV}$ so

$$R = \frac{q_2}{q_2 + q_1 \, 1.035 + q_0 \, 0.004}$$

for positive extraction, followed by charge exchange.

For direct negative extraction, the most commonly used R values are tabulated as follows:

charge change	exact R value	
$-1 \rightarrow +1$	.490	$R = 1/2$
$-1/3 \rightarrow +2/3$ or $\quad -1 \rightarrow +2$	.658	$R = 2/3 \quad -1/3 \rightarrow 2/3$ FCP search and +2 charge state are degenerate
$-1 \rightarrow +2 \rightarrow +1$	.329	Background for $-2/3 \rightarrow 1/3$ FCP search
$-2/3 \rightarrow +1/3$	.325	Setting for $-2/3 \rightarrow +1/3$ FCP search

From this table it is clear why a high resolution analysis system was required. The $-1 \rightarrow +2 \rightarrow +1$ background beam differs in R value by only 1.2% from the $-2/3 \rightarrow +1/3$ FCP search. Also, one sees that the $-1/3 \rightarrow +2/3$ search and the +2 charge state are degenerate.

Consider next the case of positive extraction followed by charge exchange

charge change	exact R value	
$+1 \rightarrow -1 \rightarrow +1$	.490	$R = 1/2$
$+1/3 \rightarrow -2/3 \rightarrow +1/3$	.325	Setting for $+1/3 \rightarrow -2/3 \rightarrow +1/3$ FCP search

To change from one beam to another one simply scales the R values. Also R scales with the terminal potential.

APPENDIX B

Pulse height Defect in Silicon and Gas ionization detectors

In this appendix, there is a discussion of the phenomenon that, in silicon and gas ionization detectors, heavy ions produce a smaller pulse height than lighter ions of the same kinetic energy. This is known as pulse height defect. It may be explained simply as follows. A charged particle entering the depletion layer of a silicon surface barrier detector or a gas ionization chamber loses energy by ionization. The pulse height observed is proportional to the energy lost due to ionization. If for some reason the particle loses energy other than by interacting with bound electrons, or if the collection of ionization energy is somehow inefficient, then clearly a pulse height defect will result.

A. The origins of pulse height defect

This phenomenon has been well studied in the case of silicon surface barrier detectors, and from these studies it is clear that there are several causes of pulse height defect.

Heavy ions slowing down in matter will lose energy partly by ionization and partly by interactions with the atomic nuclei. Clearly this latter process will result in some energy not ending up as ionization energy. At low energies the dominant energy loss mechanism is this interaction with the atomic nuclei, so-called "nuclear stopping." Calculations of the magnitude of this effect have been made by Lindhard, et al., 1968. Clearly the heavier the ion the larger this effect will be.

A second contribution to pulse height defect is incomplete charge collection in the detector. For heavy ions in a silicon detector this is principally caused by the recombination of electron-hole pairs in the plasma column produced by the heavily ionizing particle. Clearly one would anticipate that this would be much less for a gas detector as the density is much lower here than in the depletion layer of a surface barrier detector.

Another source of pulse height defect is the presence at the surface of the detector of a dead layer--the so-called "window" defect. This can be calculated from the thickness of the dead layer and the $\frac{dE}{dx}$ of the ion in that layer.

Clearly the solution to the pulse height defect problem is to send particles of known mass and energy into the detector and to calibrate it directly. This is what was done in this experiment and is described in the following section.

B. Calibration of detectors for pulse height defect

One cannot put the detectors at $0°$ in the beam as the rate will cause problems. In the case of the silicon detector, the detector will be destroyed by radiation damage. A dose of 10^{10} particles (1 nA for 2 seconds) will do this. In the case of the gas detector, the rate will be too high.

Instead, heavy ions were Rutherford-scattered off a 10 μg cm^{-2} gold foil through $90°$ into the detector. The gold foil was backed by a 20μg cm^{-2} carbon foil. The foil was inclined at $45°$ to the direction of the incoming beam. The detector was positioned at $90°$ to the beam. The +1, +2, +3, and +4 charge states of H, O, F, Al, Cl, Cu, and Nb were used to generate pulse height defect curves. The laboratory differential scattering cross-section $\frac{d\sigma}{d\Omega}$ is given by

$$\frac{d\sigma}{d\Omega} = \left\{ \frac{z_1 z_2 e^2}{4E} \right\}^2 \frac{4[(1 - \left[\frac{M_1}{M_2}\sin\theta \right]^2)^{\frac{1}{2}} + \cos\theta \ ]^2}{\sin^4\theta[1 - \left[\frac{M_1}{M_2}\sin\theta \right]^2]^{\frac{1}{2}}}$$

where

$\quad\quad Z_1 = \quad$ atomic number of projectile

$\quad\quad M_1 = \quad$ atomic mass of the projectile

$\quad\quad Z_2 = \quad$ atomic number of the target atom

$\quad\quad M_2 = \quad$ atomic mass of the target atom

$$\theta = \qquad \text{laboratory scattering angle}$$
$$E = \qquad \text{energy of incident projectile} \ .$$

The projectile energy immediately after scattering, E_f, is related to E by the kinematic factor δ

$$\delta = \frac{E_f}{E} = \left\{ \frac{[1 - \left[\frac{M_1}{M_2}\sin\theta\right]^2]^{1/2} + \frac{M_1}{M_2}\cos\theta}{1 + \frac{M_1}{M_2}} \right\}^2 .$$

Here $\theta = 90°$ so

$$\delta = \frac{M_2 - M_1}{M_2 + M_1}.$$

For silicon detectors there exists a prescription due to Kaufmann, et al., 1974 for calculating pulse height defect. The measured values agreed with this prescription at the 1-2% level. Figure 20 shows the pulse height defect data for the thin silicon detector. This prescription is in the form of a universal curve in terms of the LSS [Lindhard, et al, 1968] energy ε which is defined as

$$\varepsilon = E \frac{0.8853a_0[Z^{2/3} + Z_2^{2/3}]^{-1/2}M_2}{Z_1} Z_2 e^3 (M_1 + M_2).$$

Here a_0 is the radius of the first Bohr orbit of hydrogen. Then this universal curve is given by

$$\Delta\varepsilon(\varepsilon) = \frac{6\varepsilon}{\varepsilon + 8} + \frac{A}{1 + 525\varepsilon^{-1.407}}.$$

A is a parameter which depends on the detector. 1-2% agreement was obtained with $A = 14.0$ for a 60 μm, +100 V bias detector.

The situation with the gas detector was less clear. No published measurements existed prior to this experiment. It was possible that the pulse height defect might be significantly less because of the lower density of target particles. The nuclear stopping contribution for isobutane

turns out to be very close to that for silicon. The window effect is readily soluble as the window thickness is accurately known. The Rutherford scattering procedure was again carried out and the results shown in Fig. 22 were obtained. The pulse height defect at 2 MeV for Nb in the gas is 35% while in the silicon detector it is 45%. Thus, as expected, the gas is better but no spectacularly so.

C. Pulse Height Defect as a Measurement of Mass

Consider a beam of 2 MeV particles incident on the silicon detector. The detector gain is set so that the energy calibration is 5 keV per channel. Protons will yield a pulse height equivalent to channel 400. Heavier particles will have a significant pulse height defect and so will have a pulse height below channel 400. For example, 2 MeV copper ions will give a peak at channel 260. Uranium will give a pulse height at channel 120. Thus one obtains a mass spectrum of the beam particles. Fig. 21 shows a plot of pulse height vs. mass in amu for the thin silicon detector. The detector had a bias of + 33 V, and thus a thickness of 20 μm. The data for the gas detector are shown in Figure 23. This technique has proved very useful in the experiment. For example, when the initial spectrum at $R = 1/2$ of the direct extraction FCP source was obtained, there resulted two peaks with masses of approximately 20 and 35 amu. The high energy analyzing magnet was then tuned for these mass regions and it was discovered that the major components of the beam from the direct negative extraction FCP source were fluorine and chlorine.

This pulse height calibration of the detectors determined the size of the pulse height window required in the experiment. If one takes the region between channels 120 and 400 as the pulse height window, then one is sensitive to FCP of all masses below 240 GeV/ c^2.

APPENDIX C

The Calculation of Charge-exchange Transmission Efficiencies

In this appendix, the charge-changing transmission is calculated for the rubidium charge-exchange canal on the injector. This quantity depends on the mass, energy and electron affinity of the beam particle as well as the ionization potential and electron affinity of the rubidium target vapour. It is important to know this number, as it enters into the determination of the total transmission from sputtering site to detector, in the positive extraction search. In the analysis for FCP s, the electron affinity and ionization potential values were taken from Lackner and Zweig.

A. The theory of charge-exchange

When integrally positive keV ions are injected into a charge-exchange canal, the negative ions are formed mainly by two successive electron capture collisions with the metal vapour. The positive ions first capture one electron to form neutral atoms, and subsequently the neutral atoms capture an additional electron to form negative ions. The resulting absolute yield, $Y(q,x)$, of any positive, neutral, or negative charge states (q), is completely determined by *(i)* the charge-changing cross sections $\sigma(i,j)$ from initial charge state i to a final charge state j , *(ii)* the target vapour thickness x, and *(iii)* the initial charge state distribution $Y(q,0)$ from a system of equations given by

$$Y(q,x) = \sum_i \int_0^x \sigma(i,q) \ Y(i,z) \ dz \ -$$

$$\sum_j \int_0^x \sigma(q,j) \ Y(q,z) \ dz.$$

The cross sections for single electron transfer, *(i.e. $j = i+-1$)* are much larger than those for double or multiple electron transfer. As the thickness is increased beyond a certain point, $Y(q,x)$ are no longer dependent

on x, i.e.,

$$\frac{dY}{dx}(x=x_e) = 0$$

and an equilibrium charge state distribution is reached. Let the normal-ized equilibrium charge state fraction be F(q) so

$$F(q) = \frac{Y(q, x \gtrsim x_e)}{\sum_q Y(q, x \gtrsim x_e)}.$$

Because the multiple electron transfer cross sections are small, we have

$$\frac{F(q)}{F(q+1)} = \frac{\sigma(q+1 \to q)}{\sigma(q \to q+1)}.$$

In the case of keV ions, the neutralization cross section, $\sigma(+1 \to 0)$, is typically much larger than the ionization cross section, $\sigma(0 \to +1)$, so $F(+1) << F(0)$. Thus at equilibrium, only two charge states are dominant; 0 and -1.

The behavior of electron capture and loss cross sections can be understood in a theory which uses the pseudo-crossing of energy-levels [cf. Landau 1932, Zener 1932]. Consider $+1/3 \to -2/3$ and $-2/3 \to +1/3$ charge-change in the rubidium vapor. The initial molecu-lar potential energy curve is dominated by the weak polarizing force between the charged FCP beam particle and the neutral rubidium target atom. The final interatomic potential curve is dominated by the strong Coulomb force between the charged products - the FCP and rubidium ions. If these potential curves cross at a nuclear separation R, then it can be shown [cf. Bates 1954] that the charge changing cross-section is

$$\sigma = 4 \pi R^2 I(\eta)$$

where

$$R = \frac{q_1 q_2}{\Delta E}$$

$q_1 q_2 = $ charges of end-products

$\Delta E =$ energy defect

$$\eta = \frac{4\pi^2 q_1 q_2 \sqrt{M}\, \Delta U(R)^2}{h\, \Delta E^2 E^{0.5}\sqrt{2}}$$

$M =$ reduced mass

$E =$ center of mass energy

$v =$ relative velocity

$\Delta U(R) =$ separation of the potential energy curves at the pseudo-

crossing

$$I(\eta) = \int\limits_{1}^{\infty} e^{-\eta x}\left[1 - e^{-\eta x}\right]\frac{dx}{x^3}$$

$I(\eta)$, when plotted as a function of $\log \eta^{-2}$, is a bell-shaped curve having a maximum of 0.113 at $\eta = 0.424$ [cf. Boyd 1957]. η is inversely proportional to the velocity. The maximum value of η corresponds to a value of the velocity ,v_{max} , at which the charge changing cross-section is a maximum. This is

$$v_{max} = \frac{4\pi^2 q_1 q_2 \Delta U(R)^2}{0.424 h\, \Delta E^2}.$$

This maximum velocity is also approximated by the Massey adiabatic condition

$$v_{max} = a\frac{\Delta E}{h}.$$

This is obtained by demanding that the interaction time be comparable to the transmission time. Here a $\sim 3\ A^0$ for these types of electron transfer processes [cf. Hasted 1960]. Further, one can show that

$$\sigma\left(\frac{v}{v_{max}}\right) = 4\pi\, I\left(\frac{v}{v_{max}}\right)\left[q_1\frac{q_2}{\Delta E}\right]^2.$$

B. The calculation of transmission efficiencies

Consider the case $+1/3 \to -2/3$. We have

$$\frac{F(-2/3)}{F(+1/3)} = \frac{\sigma(+1/3 \to -2/3)}{\sigma(-2/3 \to +1/3)},$$

so, to calculate $F(-2/3)$, we must determine $\sigma(+1/3 \to -2/3)$ and $\sigma(-2/3 \to +1/3)$ as a function of mass, using the procedure outlined above. One first determines

$$v_{max} = a\frac{\Delta E}{h}$$

where $\Delta E = (4.16 - 1.5)\, eV$ is the difference between the rubidium ionization potential and the $Z = 1/3$ electron affinity. This v_{max} determines an M_{max} where

$$M_{max} = 2\,\frac{8}{3\,v_{max}^2}.$$

M_{max} is the mass of an FCP with energy $\frac{8}{3} keV$ which has velocity v_{max}. One can then consider a $+1/3$ FCP of arbitrary mass m and determine $\frac{v}{v_{max}}$ for it. Then

$$\eta = 0.424\,\frac{v}{v_{max}},$$

and $I\left(\frac{v}{v_{max}}\right)$ can be determined from the bell-shaped curve. Hence,

$$\sigma\left(\frac{v}{v_{max}}\right) = 4\pi I\left(\frac{v}{v_{max}}\right)\left[q_1\frac{q_2}{\Delta E}\right]^2$$

can be determined. We now have $\sigma\left(\frac{v}{v_{max}}\right)$ as a function of mass for the $+1/3 \to -2/3$ process.

One then repeats the procedure for $-2/3 \to +1/3$. Here $\Delta E = 1.5 - 0.52\, eV$ is the difference in electron affinities of the $+1/3$ FCP and the neutral rubidium atom. One ends up with $\sigma\left(\frac{v}{v_{max}}\right).(v_{max}$

is different for this process), as a function of mass for the $-2/3 \rightarrow +1/3$ process. One can then determine $F(-2/3)$ and $F(+1/3)$ using

$$\frac{F(-2/3)}{F(+1/3)} = \frac{\sigma(+1/3 \rightarrow -2/3)}{\sigma(-2/3 \rightarrow +1/3)}$$

and

$$F(-2/3) + F(+1/3) = 1.$$

These results are tabulated as follows:

$\dfrac{\text{MASS}}{\text{GeV}/c^2}$	$\sigma(+1/3 \rightarrow -2/3)$	$\sigma(-2/3 \rightarrow +1/3)$	F(-2/3)
0.3	0.036	0.029	55%
1	0.052	0.051	51%
10	0.087	0.116	43%
13	0.087	0.128	40%
100	0.059	0.160	27%
250	0.030	0.145	17%

The major component of the positive extraction beam from the FCP source was found to be carbon with an electron affinity of 1.25 eV. If one carries out a similar analysis to the above in this case, one obtains a charge state transmission to the -1 state of 15%. This is in reasonable agreement with the experimentally observed value of 20%.

References

Bates,D.R.,Massey,H.S.W. 1954, Phil. Mag. **45**, 111

Boyd,T.J.M.,Moiseiwitsch,B.L. 1957, Proc. Phys. Soc. (London) **A70**, 809

Dylla,H.F.,King,J.G. 1973, Phys. Rev. A **7**, 1224

Gallinaro,G.,Marinelli,M.,Morpurgo,G. 1977, Phys. Rev. Lett. **38**, 1255

Gell-Mann,M. 1964, Phys. Lett. **8**, 214

Hasted,J.B. 1960, Adv. in Electronics and Electron Physics **13**, 1

Herrmannsfeldt,W.B. **Electron Trajectory Program**, SLAC-Report-226, 1979

Jones,L.W. 1977, Rev. Mod. Phys. **49**, 717

Kaufmann,S.B., et al. 1974, Nucl. Instr. and Meth. **115**, 47

Lackner,K.S.,Zweig,G. 1983, Phys. Rev. **D28**, 1671

Landau, L. 1932, Physik Z. Sowjetunion **2**, 46

LaRue,G.S.,Fairbank,W.M.,Hebard,A.F. 1977, Phys. Rev. Lett. **38**, 1011

LaRue,G.S.,Fairbank,W.M.,Phillips,J.D. 1979, Phys. Rev. Lett. **42**, 142

LaRue,G.S.,Phillips,J.D.,Fairbank,W.M. 1981, Phys. Rev. Lett. **46**, 967

Lindhard,J.,Nielson,V.,Sharff,M. 1968, Mat. Fys. Medd. Dan. Vid. Selsk **36**, no. 10

Morgan III,J.D.,Barnhill III,M.V. 1983, Phys. Lett. **133B**, 227

Northcliffe,L.C.,Schilling,R.F. 1970, Nucl. Data **A7**, 233

Sigmund,P. 1969, Phys. Rev. **184**, No. 2, 383

Slansky,R.,Goldman,T.,Shaw,G.L. 1981, Phys. Rev. Lett. **47**, 887

Wittkower,A.B.,Ryding,G. 1971, Phys. Rev. A **4**, 226

Wollnick,H.,Ewald,H. 1965, Nucl. Instr. and Meth. **36**, 93

Zeigler,J.F., **Handbook of Stopping Cross-Sections for Energetic Ions in All Elements**, vols 1-5 (Pergamon, New York, 1980)

References (contd.)

Zener,C. 1932, Proc. Roy. Soc. (London) **A137**, 696

Zweig,G. 1964, CERN Report **8419**/TH.412

Zworykin,V.K.,Morton,G.A.,Ramberg,E.G.,Hillier,J.,Vance,A.W.   **Electron Optics and the Electron Microscope**, (Wiley, New York, 1948)

Table 1

Table 1 indicates the integral and peak counts for niobium and tungsten in the search for $Z = N + 1/3$, $EA \gtrsim 3.5\text{eV}$ particles.

$R = 1/3$, direct negative extraction

material	stripper gas	Z	running time	energy window	counts
			hours	MeV	integral : peak
Nb	H_2	$N + 1/3; N = 1,2,..$ $EA \gtrsim 3.5eV$	41.6	0.65 - 2.05	271 : 15
W	H_2	$N + 1/3; N = 1,2,..$ $EA \gtrsim 3.5eV$	7.38	0.65 - 2.05	278 : 81

Table 2

Table 2 summarizes the upper limits obtained for FCP concentrations in the niobium target.

Niobium concentration limits

Z	MASS GeV/c^2	FCP/NIOBIUM ATOM	
		PEAK	INTEGRAL
$\dfrac{1}{3}$	$0.2 \lesssim m \lesssim 250$	see Figure 15	
$\dfrac{2}{3}$	$0.2 \lesssim m \lesssim 250$	2.2×10^{-17}	
$\dfrac{4}{3}$	$0.3 \lesssim m \lesssim 14$	5.2×10^{-19}	
$\dfrac{5}{3}$	$0.2 \lesssim m \lesssim 4$	4.9×10^{-18}	
$N + 1/3$[a]	$0.7 \lesssim m \lesssim 250$	1.5×10^{-18}	2.8×10^{-17}
$N + 1/3$[b]	$0.7 \lesssim m \lesssim 250$	see Figure 18	1×10^{-17}

[a] N=1,2,3,... and electron affinity $\gtrsim 3.5\ eV$; negative extraction.

[b] N=1,2,3,... and electron affinity $\lesssim 3.5\ eV$; positive extraction
with Rubidium charge exchange.

Table 3

Table 3 summarizes the upper limits obtained for FCP concentrations in the tungsten target.

Tungsten concentration limits

Z	MASS GeV/c^2	FCP/TUNGSTEN ATOM	
		PEAK	INTEGRAL
$\dfrac{1}{3}$	$0.2 \lesssim m \lesssim 250$	see Figure 16	
$\dfrac{2}{3}$	$0.2 \lesssim m \lesssim 250$	1.2×10^{-16}	
$\dfrac{4}{3}$	$0.3 \lesssim m \lesssim 14$	5.9×10^{-18}	
$\dfrac{5}{3}$	$0.2 \lesssim m \lesssim 4$	1.3×10^{-17}	
$N + 1/3^{(a)}$	$0.7 \lesssim m \lesssim 250$	1×10^{-16}	4×10^{-16}
$N + 1/3^{(b)}$	$0.7 \lesssim m \lesssim 250$	see figure 19	2.5×10^{-17}

[a] $N = 1,2,3,...$ and electron affinity $\gtrsim 3.5$ eV ; negative extraction.

[b] $N = 1,2,3,...$ and electron affinity $\lesssim 3.5$ eV ; positive extraction
with Rubidium charge exchange.

Figure 1

Figure 1 is taken from LaRue, Phillips and Fairbank 1981. It presents a summary of the published data of the Stanford group.
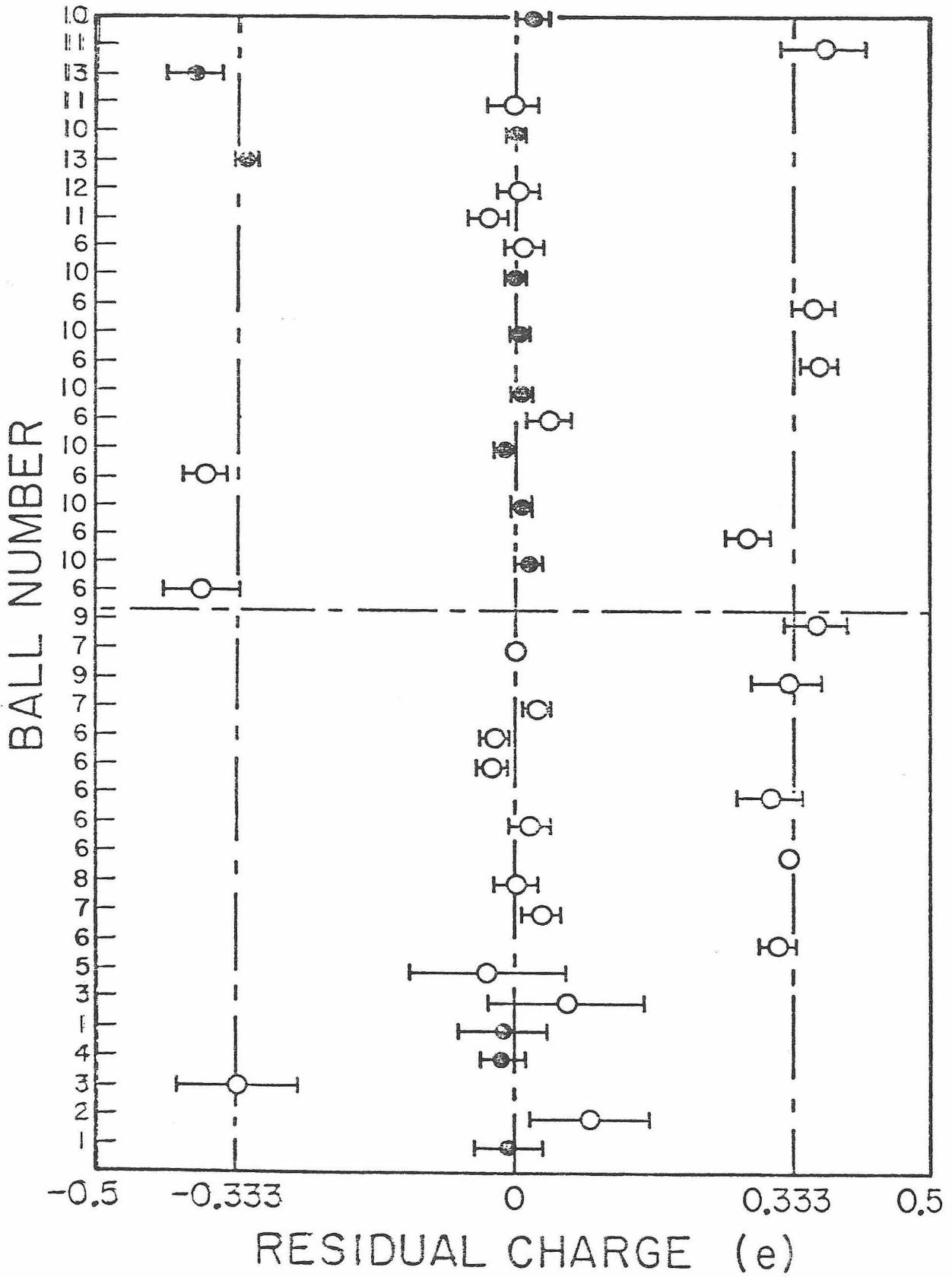
Figure 2

Figure 2 is a general schematic showing the layout of the experiment.

FCP sputter source

charge exchange canal (optional)

Cesium sputter source

accelerator tank

gas stripper

analyzing magnet (degaussed)

detector station

6m drift

two stages of electrostatic analysis

electrostatic quadrupole lens

injection magnet (degaussed)

30° cylindrical electrostatic analyzer
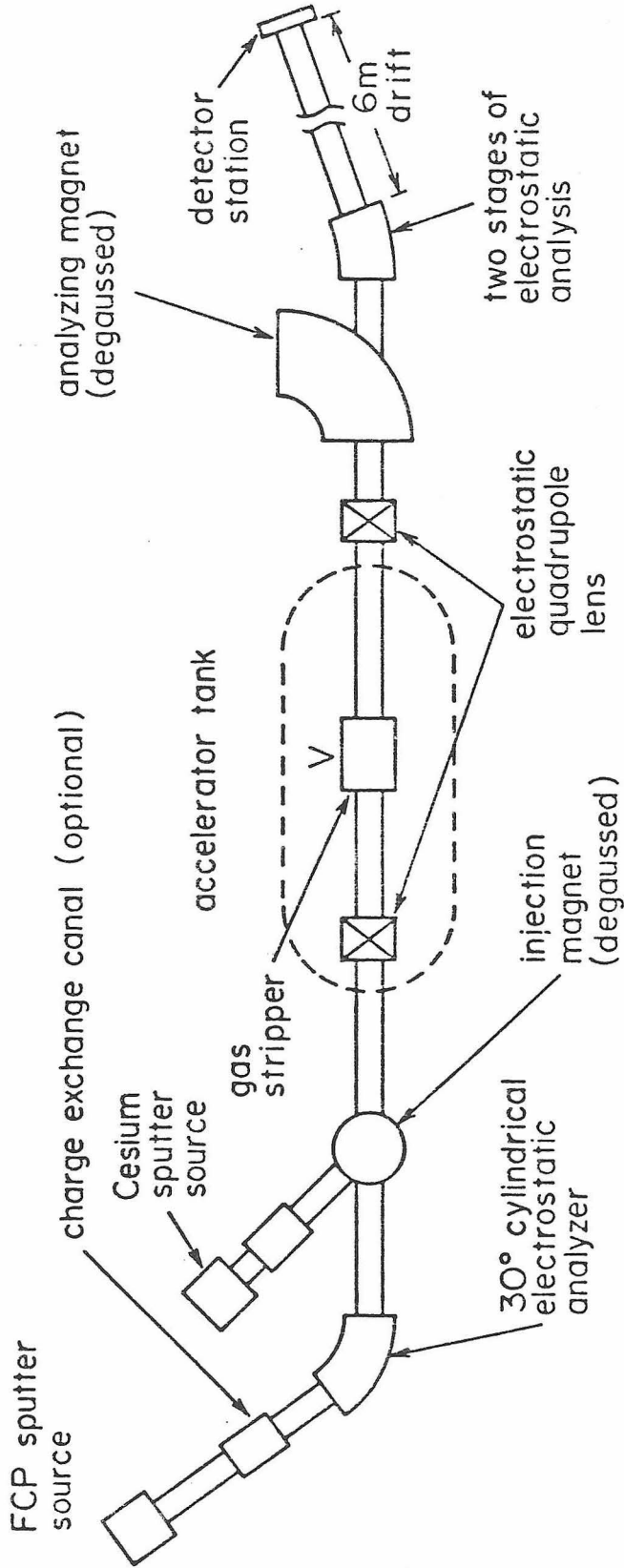
Figure 3

Figure 3 is a general schematic diagram, showing the layout of the Argon sputtering section of the FCP source.

target chamber

Einzel lens
L3

valve

cold trap

.32 cm dia. copper
aperture

30°
dipole
magnet

B field

2.54 cm dia pipe

ion
gauge
IG1

pump
out
port

CTI
8

Einzel
lens
L2

valve

50cm

G.I. 2490 Einzel
L I lens

358 G.I.
duoplasmatron
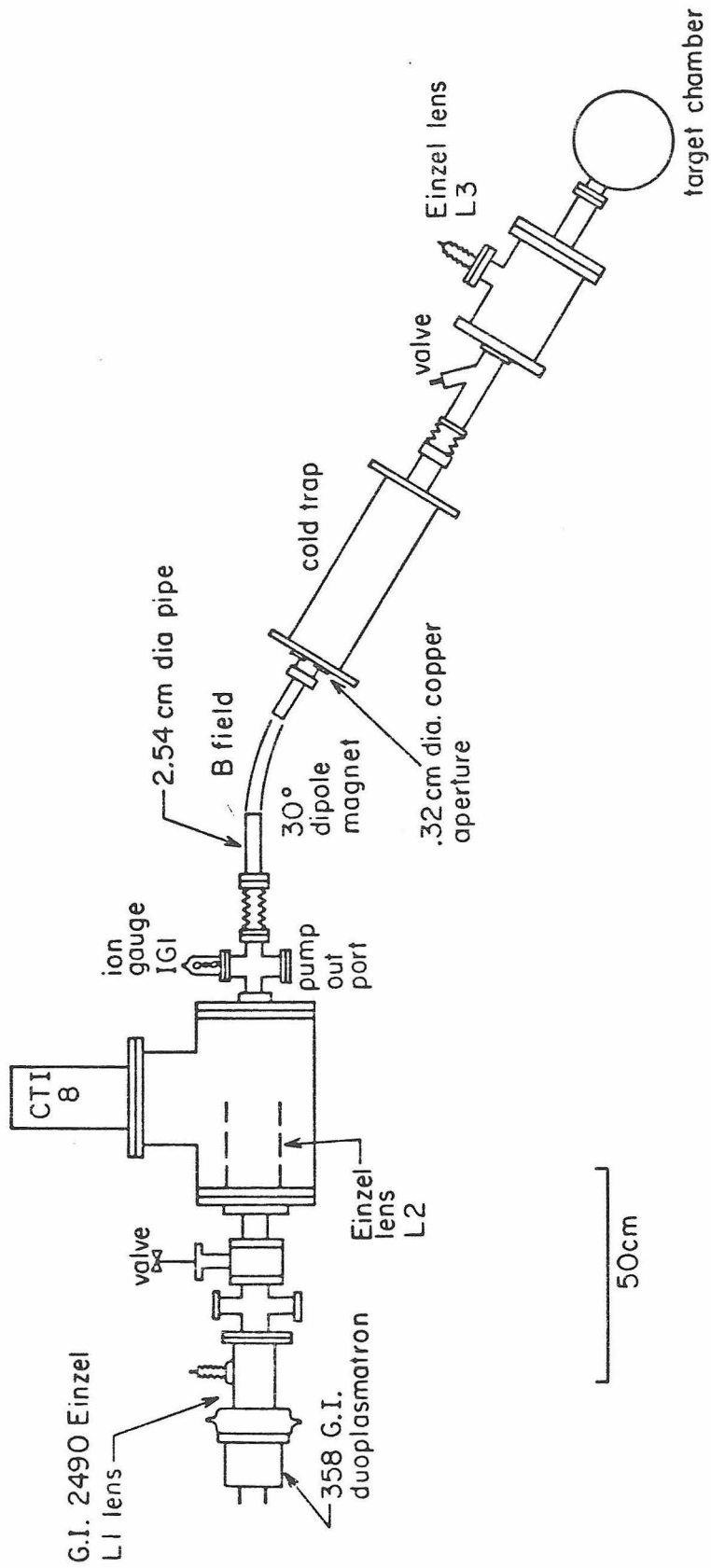
Figure 4

Figure 4 is a diagram of the target chamber and extraction geometry.
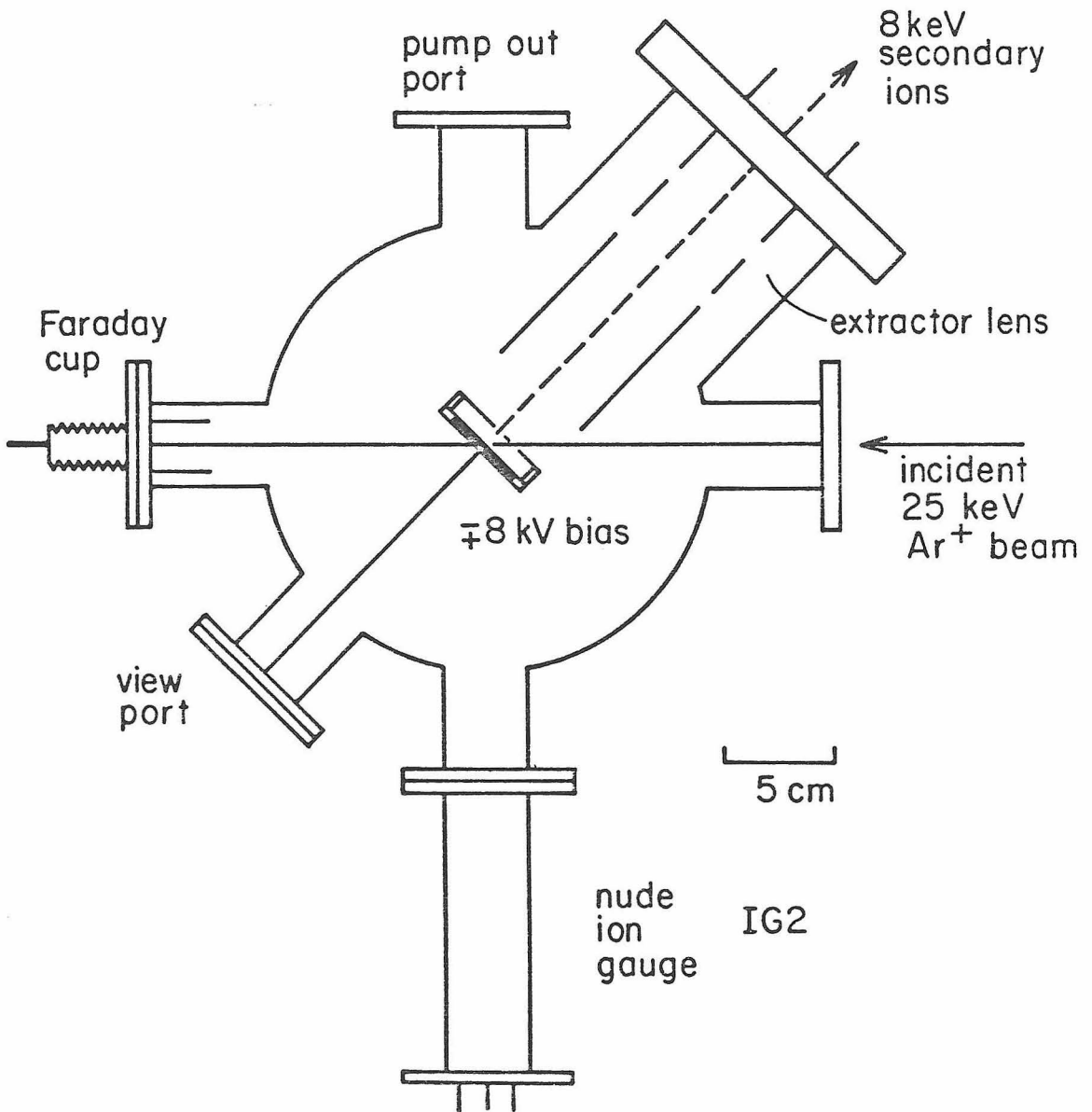
Figures 5a and 5b

Figure 5a shows some of the output rays generated by the Herrmannsfeldt program for the extraction geometry. Figure 5b is a schematic of the extraction geometry.

(a)

Argon sputter beam

sputtered ion trajectories

Einzel lens

$V_1 \approx 8kV$
$V_2 \approx 7.8kV$

Niobium target

$\mp V_1$

$\mp V_2$

(b)

E

T

d

2c

X

+V
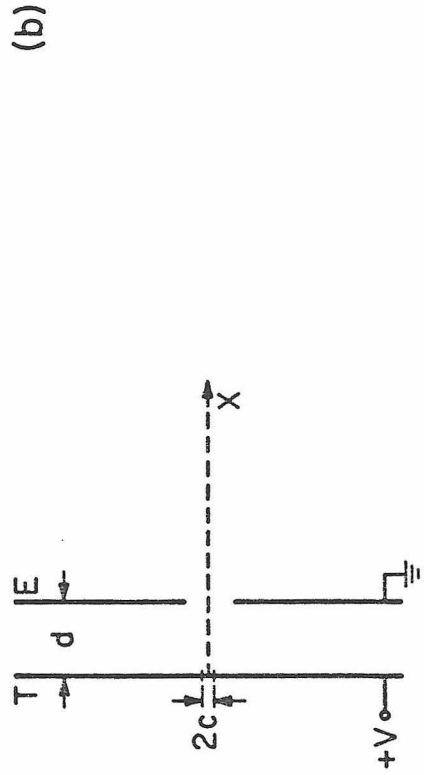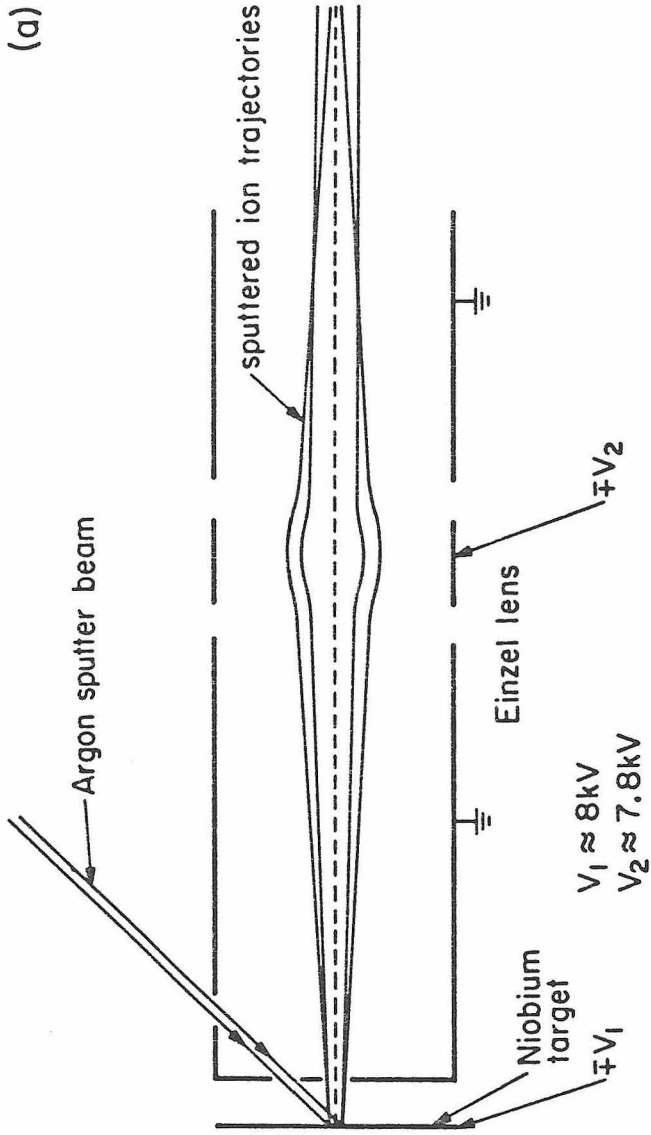
Figure 6

Figure 6 is a schematic diagram of the layout of the injector on the FCP source.

bucking coils
around chamber
field < .1 gauss

incident Ar beam →

extractor
lens

target
chamber
$\begin{pmatrix} \text{cryopump} \\ \text{beneath} \end{pmatrix}$

charge
exchange
canal →

15° electrostatic
analyzer

accelerating
column

sputtered
ions

injector Einzel lens

30° electrostatic
analyzer $\begin{pmatrix} \text{cryopump} \\ \text{beneath} \end{pmatrix}$

G. I.
sputter
source

turbopump

inflection (degaussed)
magnet

1 m

turbopump

accelerator
tank

Figure 7

Figure 7 shows the layout of the high energy analysis system.

turbopump

electrostatic
quad. doublet

horizontal and vertical
magnetic steering

object slits SI
horizontal and vertical

90° analyzing magnet
(degaussed)

cryopump

1st stage

ℓ = 30 cm

d = 3 cm

θ = 2 1/2°

+V   −V

horizontal slits S2

1 m

1.25 cm slit

F1 cryopump
beneath

2nd stage

ℓ = 50 cm

d = 3 cm

θ = 8°

horizontal slits S3

5.3m ∼

F2
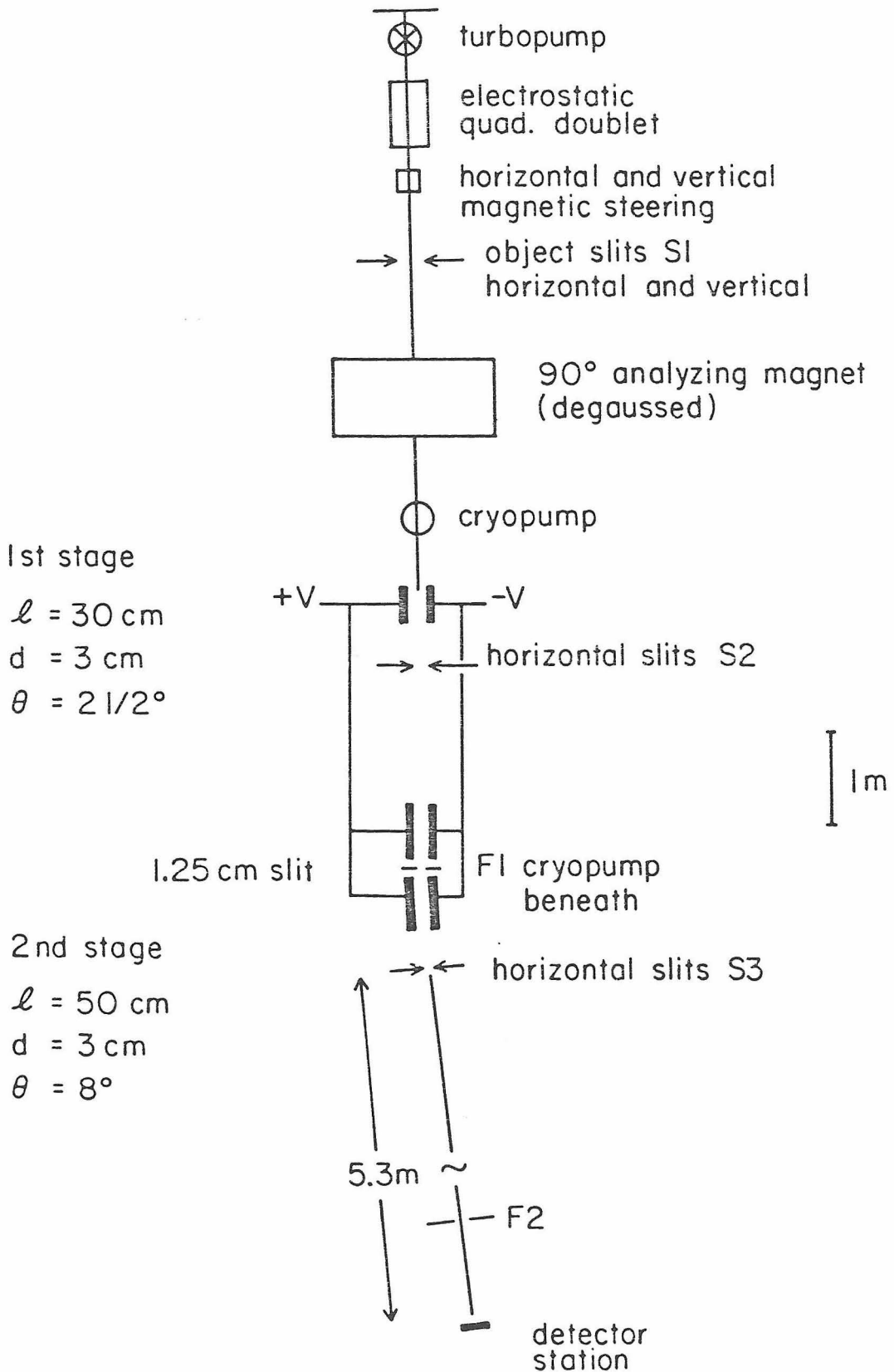
detector
station

Figure 8

Figure 8 shows the layout of the FCP detector station.

Si detector
4-way cross

uhv valve

liquid nitrogen
cold trap

2.54 cm
collimator

beam profile
monitor

5 cm

2.54 cm
collimator

Faraday
cup

^{241}Am source
on moveable
copper rod

4-way
cross

rough
out
port

insulating piece
1 cm dia. entrance window

gas
lines

in

out

gas detector
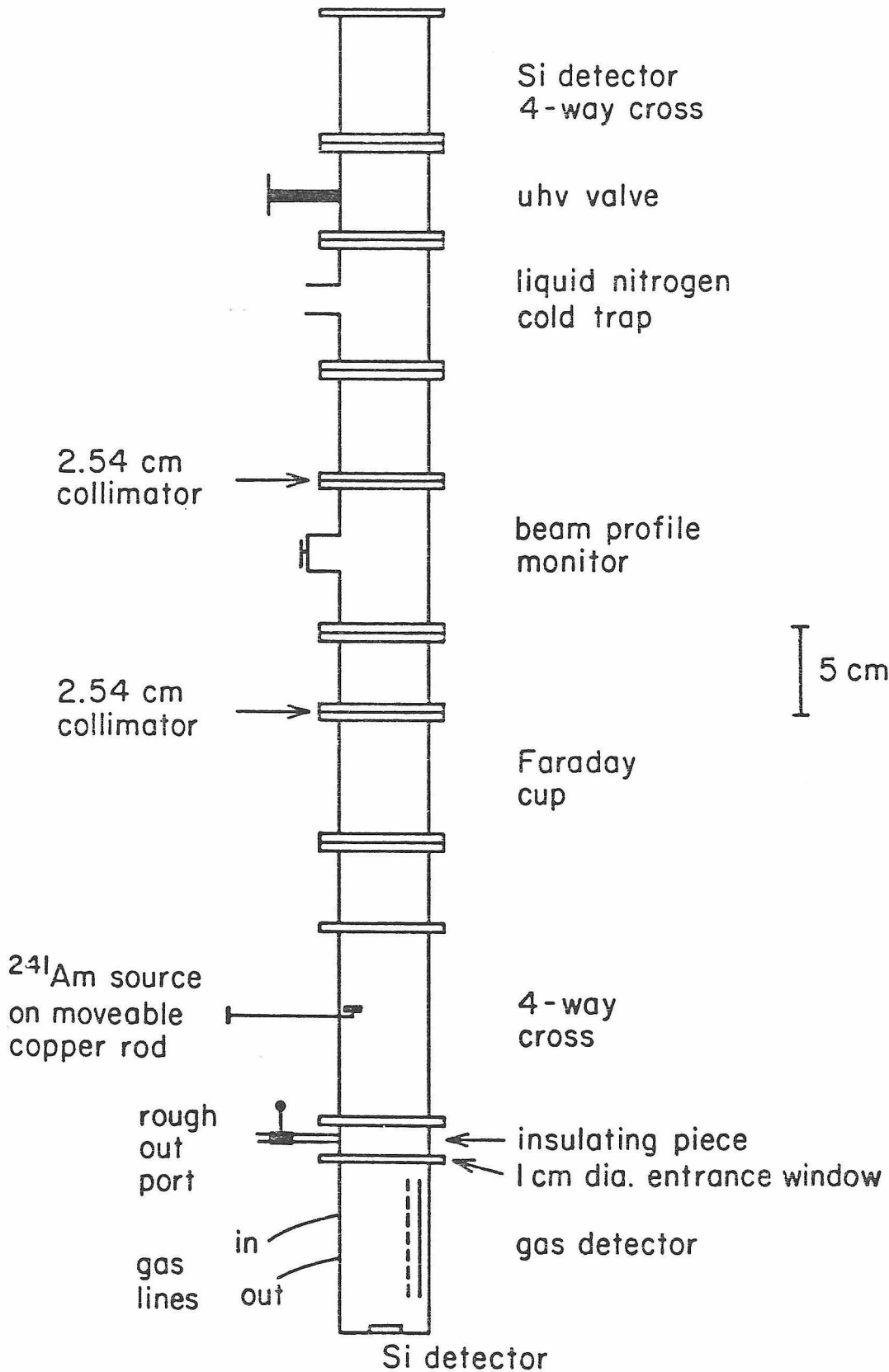
Si detector

Figure 9

Figure 9 is a 90 hour spectrum of cosmic-ray generated events in the 500 μm thick silicon detector. The events have the well known Landau distribution shape.
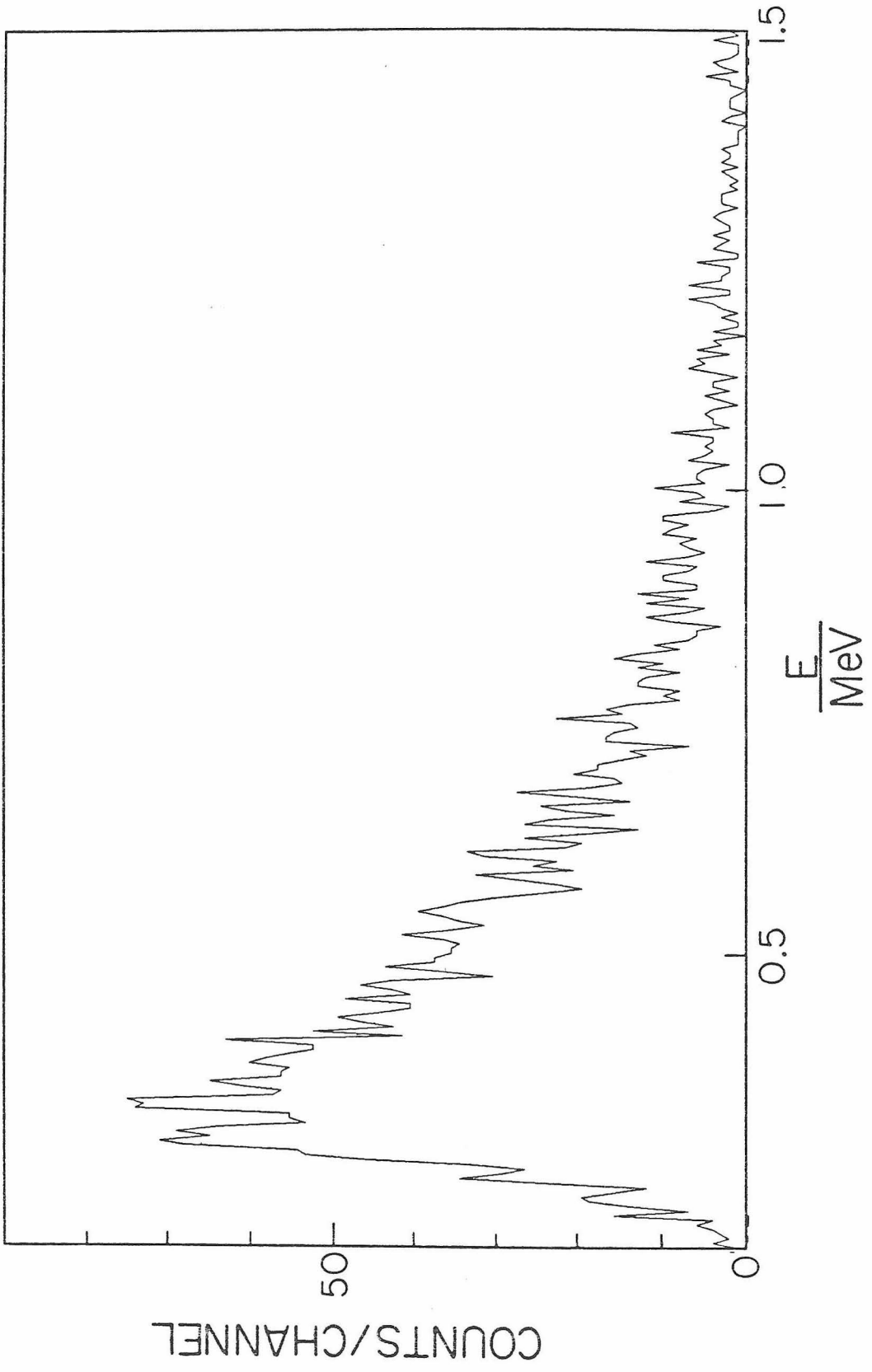
Figure 10

Figure 10 is a schematic diagram of the electronics layout.
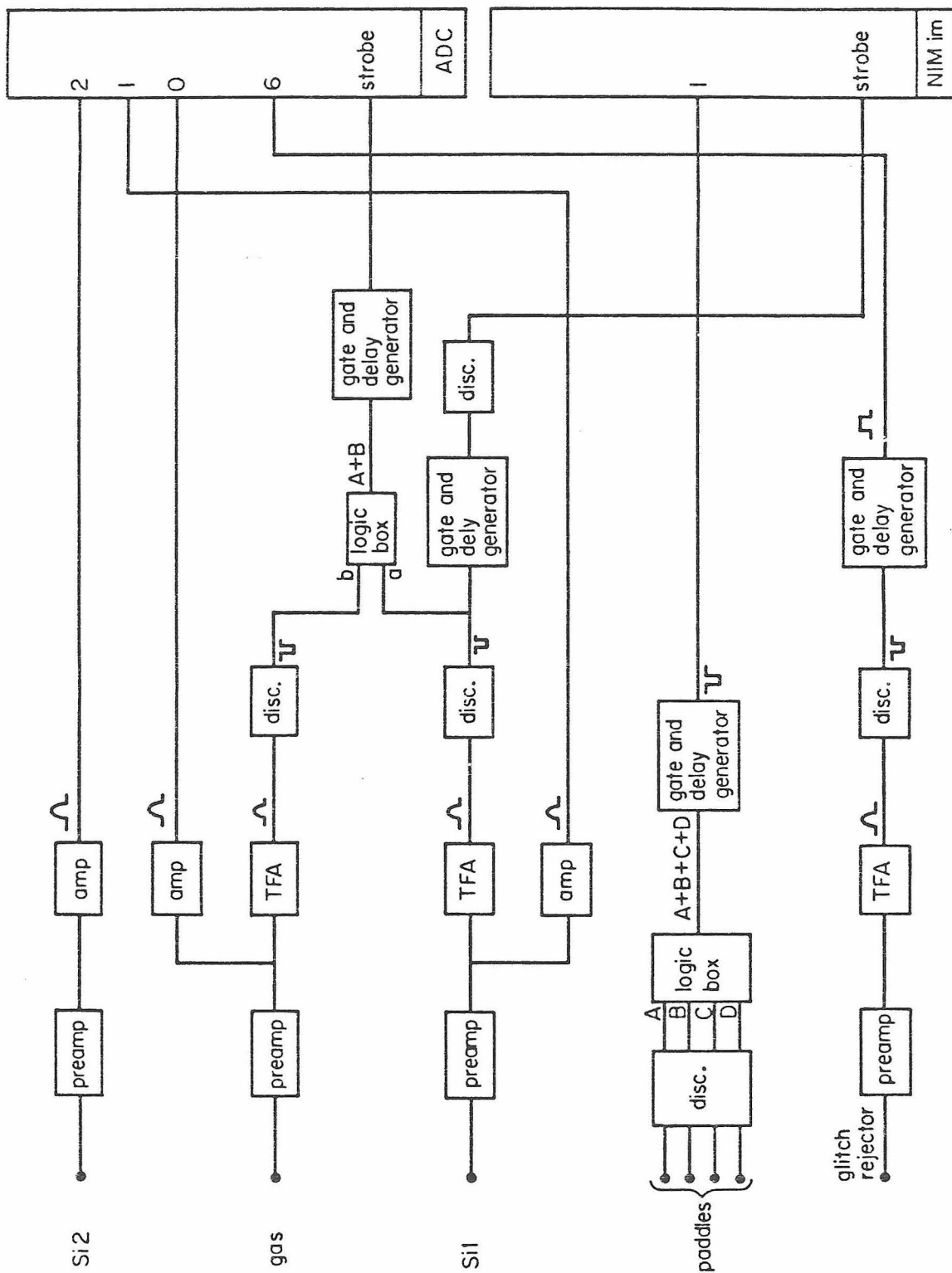
Figure 11

Figure 11 is an energy spectrum taken with the FCP source in the direct negative extraction mode and the high energy analysis system tuned for $R = 1/2$.
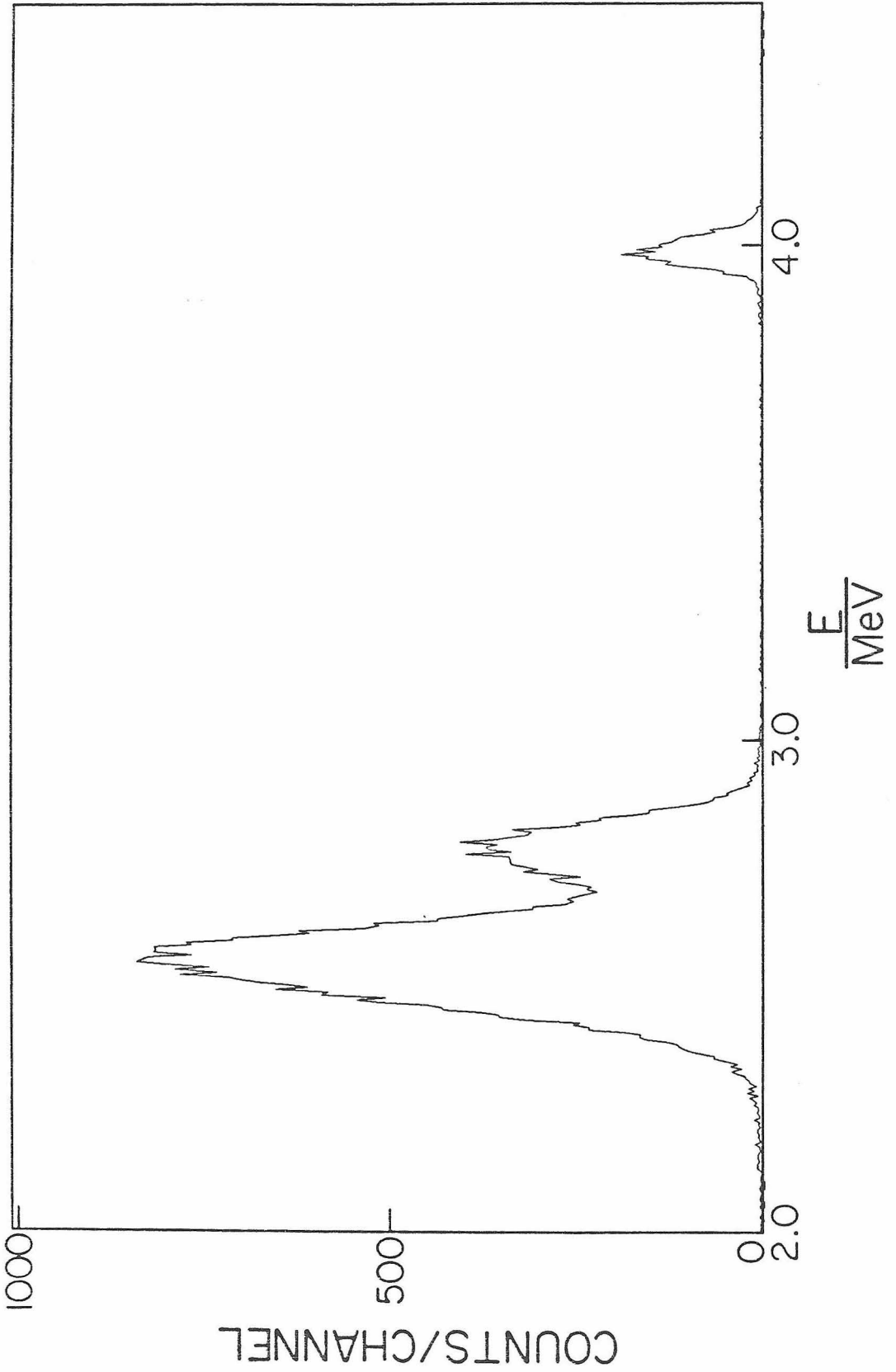
Figure 12

Figure 12 is an energy spectrum taken with the FCP source in the positive extraction mode and the high energy analysis system tuned for $R = 1/2$.
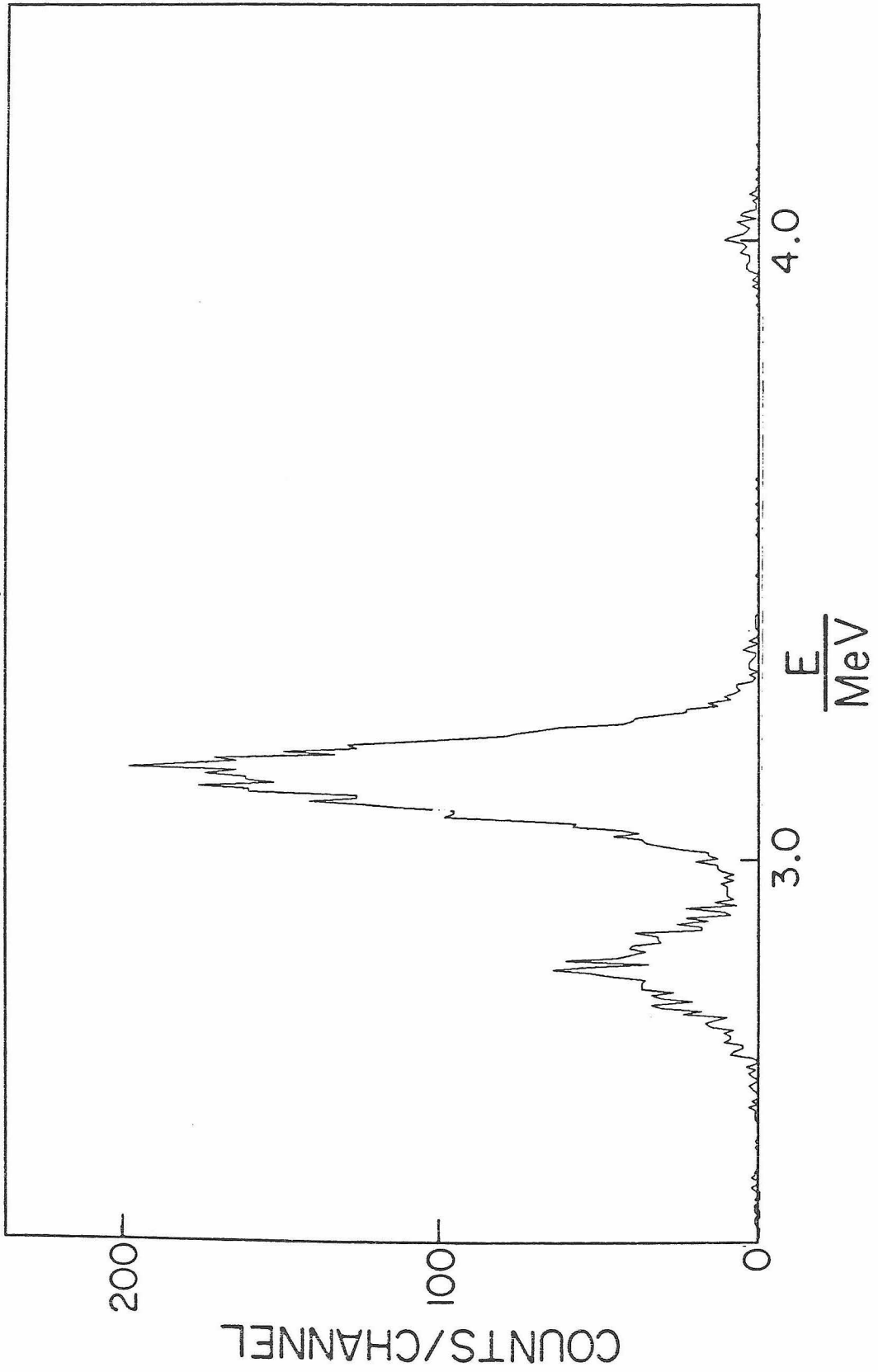
Figure 13

Figure 13 shows the energy spectrum for the niobium data for $Z = N + 1/3$, EA $\gtrsim 3.5\ eV$ particles.
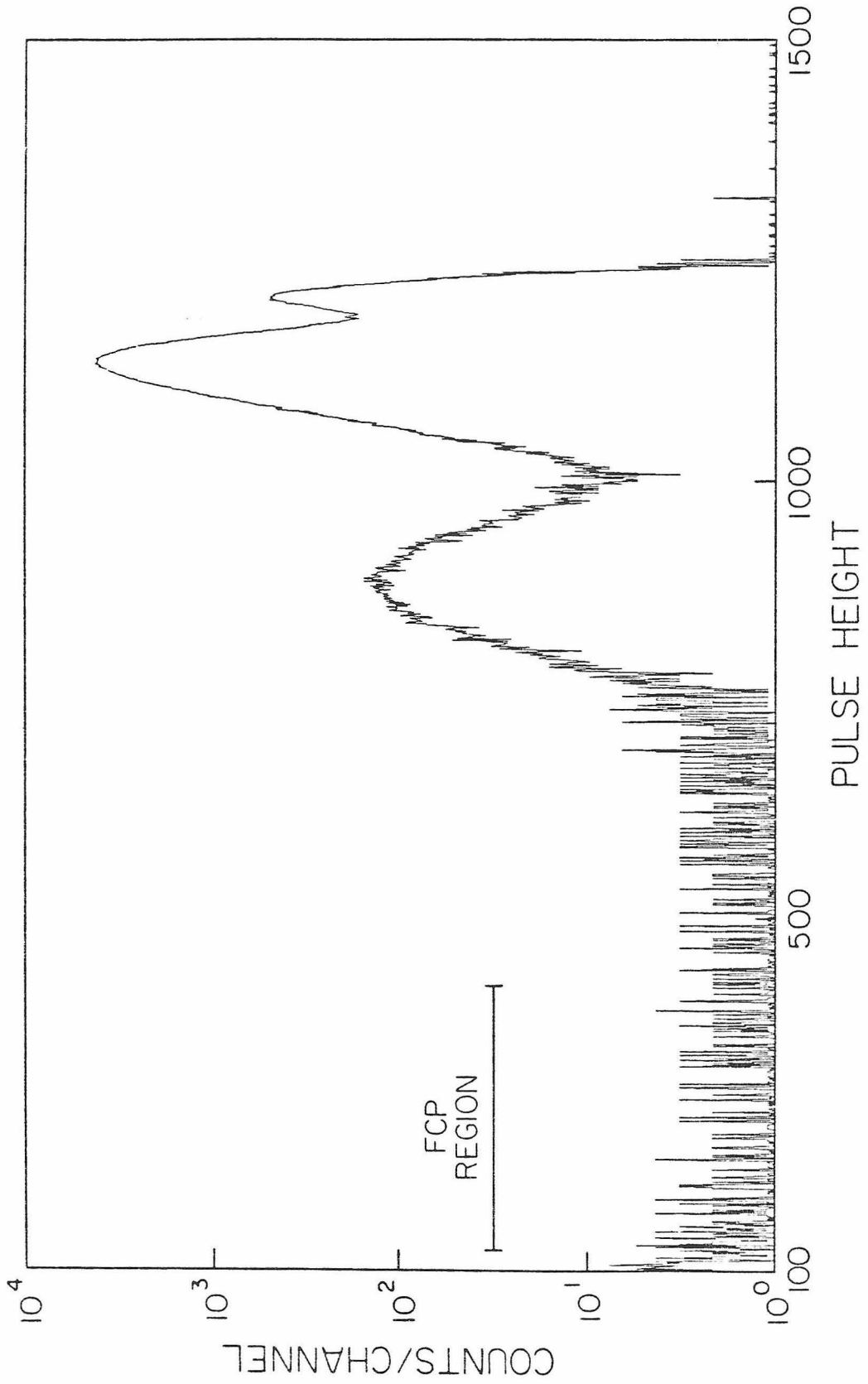
Figures 14a and 14b

Figure 14a shows the FCP region of Figure 13 enlarged. For comparison, Figure 14b shows the 2 MeV Rutherford scattered peak of niobium ions, scattered through 90° from a 10 μgcm^{-2} gold foil.
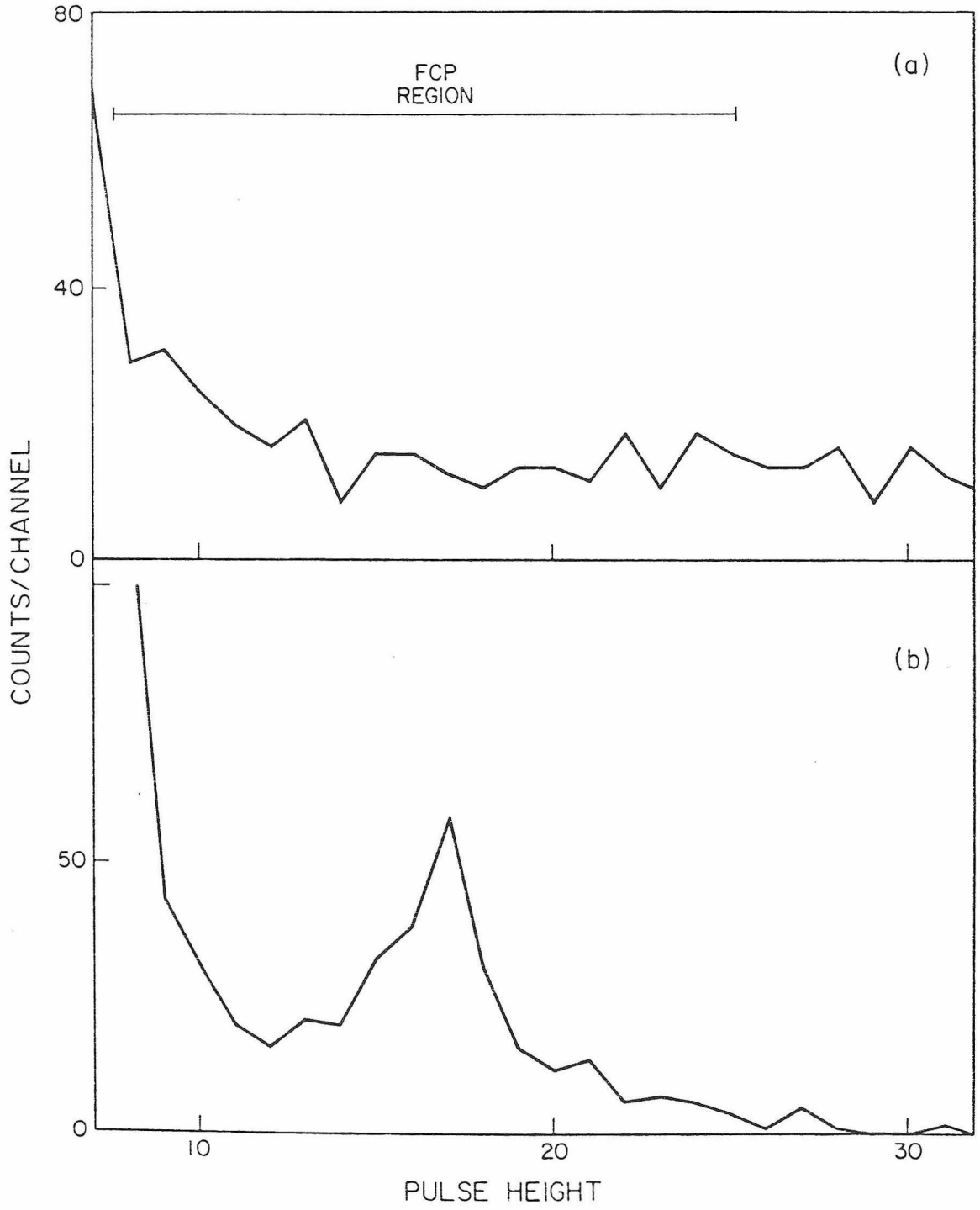
Figure 15

Figure 15 shows the measured upper limit FCP concentration per target atom in niobium plotted as a function of FCP mass for $Z = 1/3$ particles.
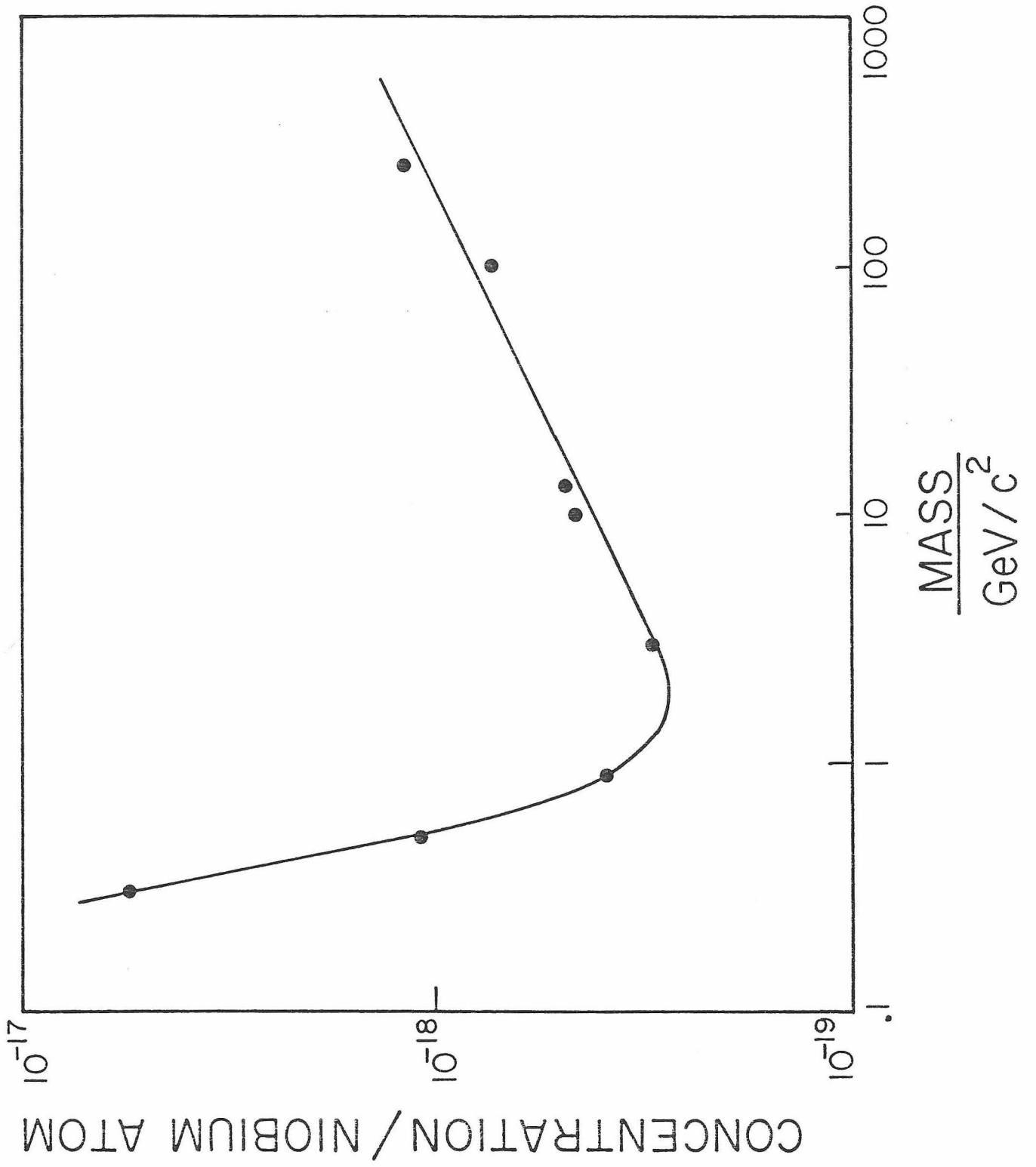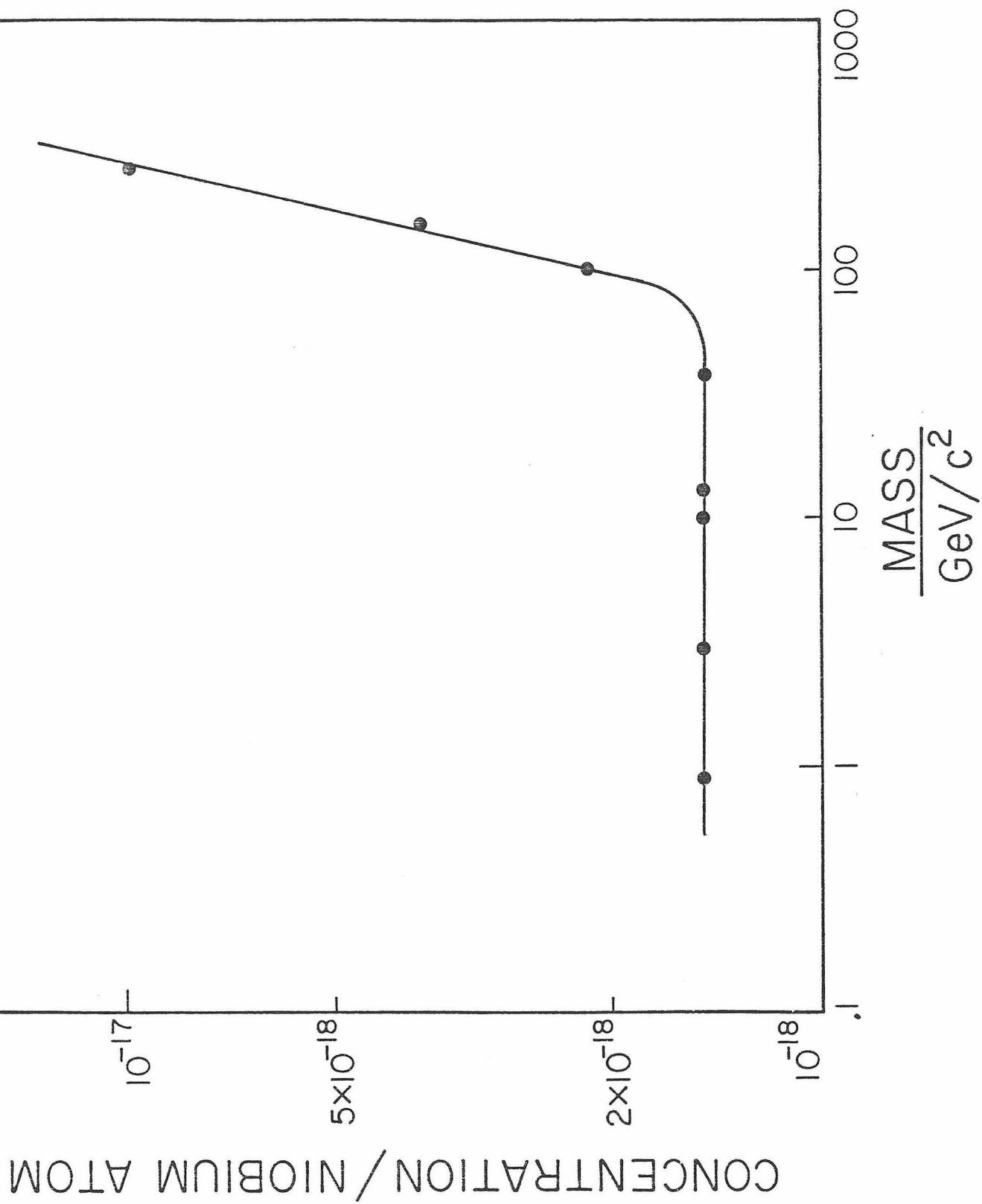
Figure 16

Figure 16 shows the measured upper limit FCP concentration per target atom in tungsten plotted as a function of FCP mass for $Z = 1/3$ particles.
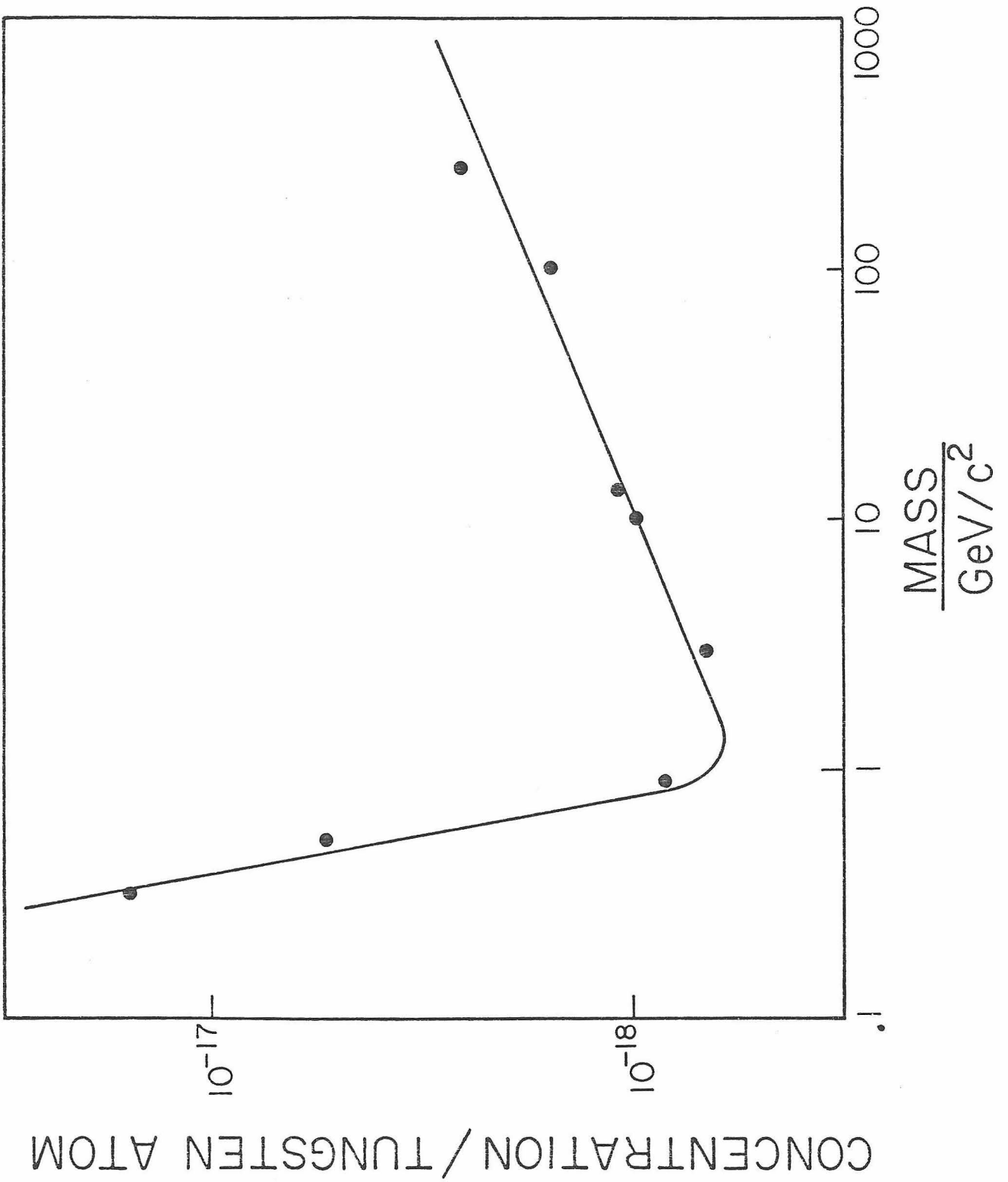
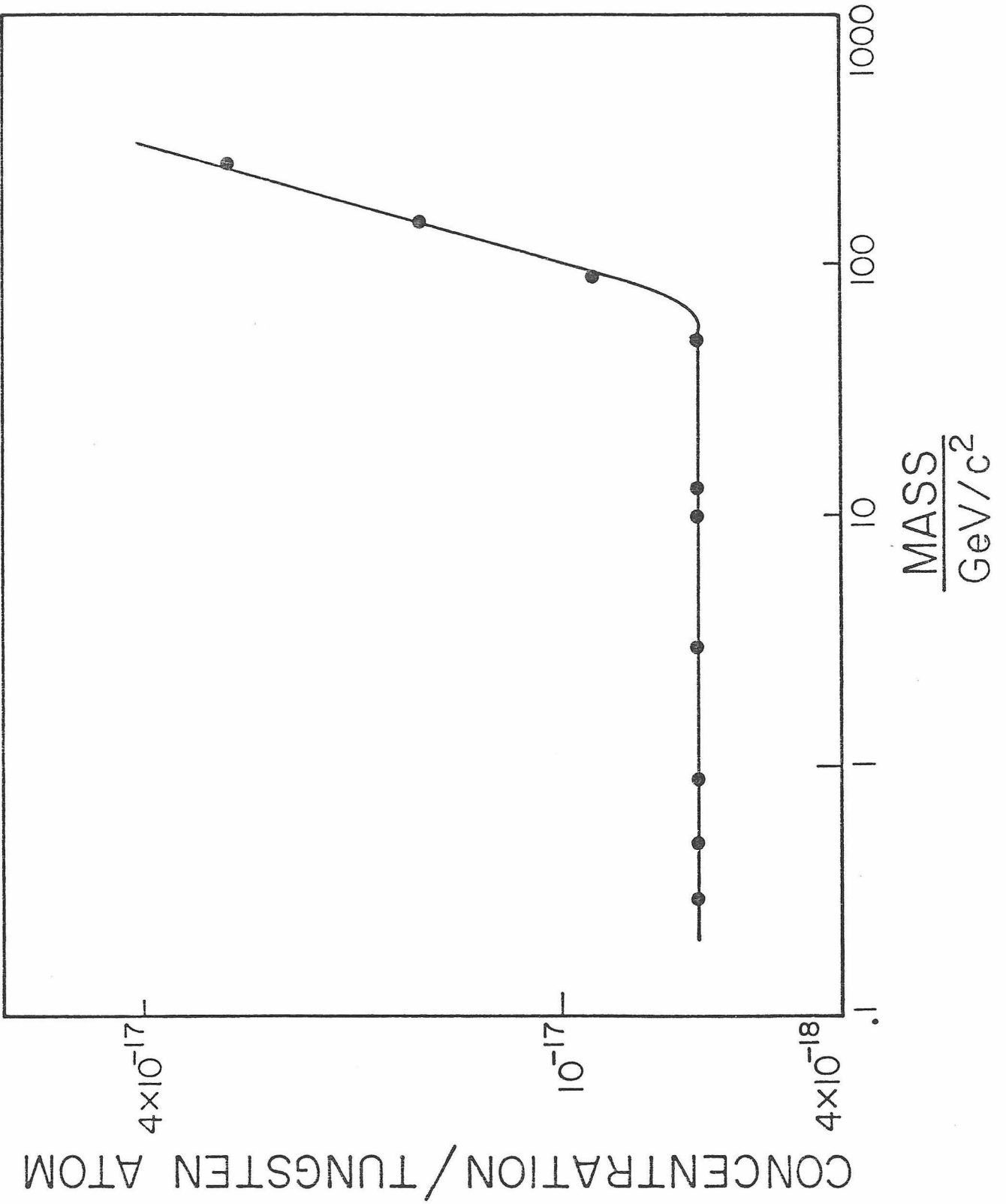# Figure 17

Figure 17 shows the background subtracted data for $Z = N + 1/3$ niobium.
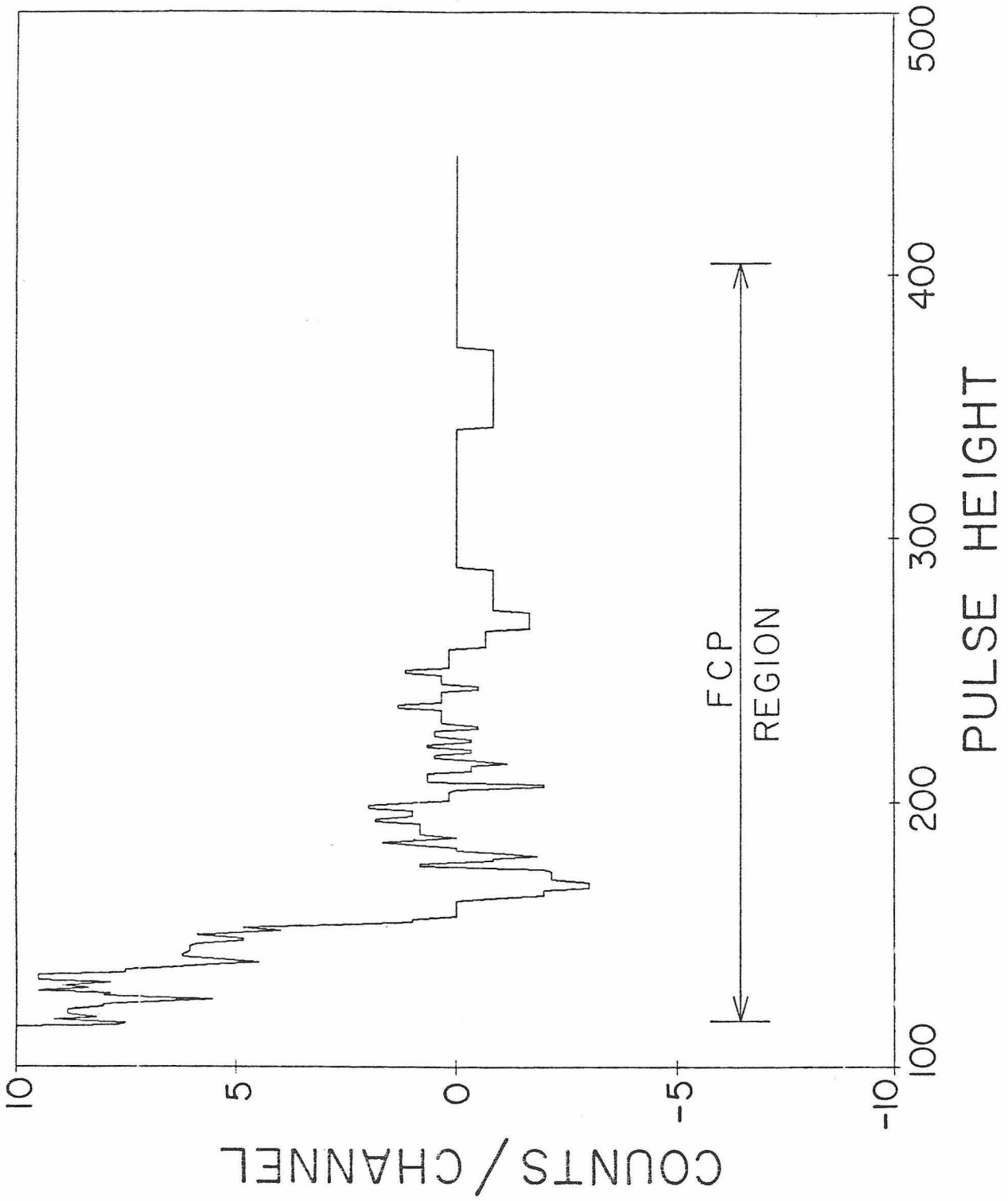
Figure 18

Figure 18 shows the measured upper limit FCP concentration per target atom in niobium plotted as a function of FCP mass for $Z = N + 1/3$ particles.

Figure 19

Figure 19 shows the measured upper limit FCP concentration per target atom in tungsten plotted as a function of FCP mass for $Z = N + 1/3$ particles.

Figure 20

Figure 20 is a plot of pulse height vs. energy for atoms of different masses for the thin silicon detector. The detector was operated at a bias of +33 V and a depletion depth of 20 μm. These data were obtained by Rutherford scattering through 90° off a 10 μgcm^{-2} gold foil.
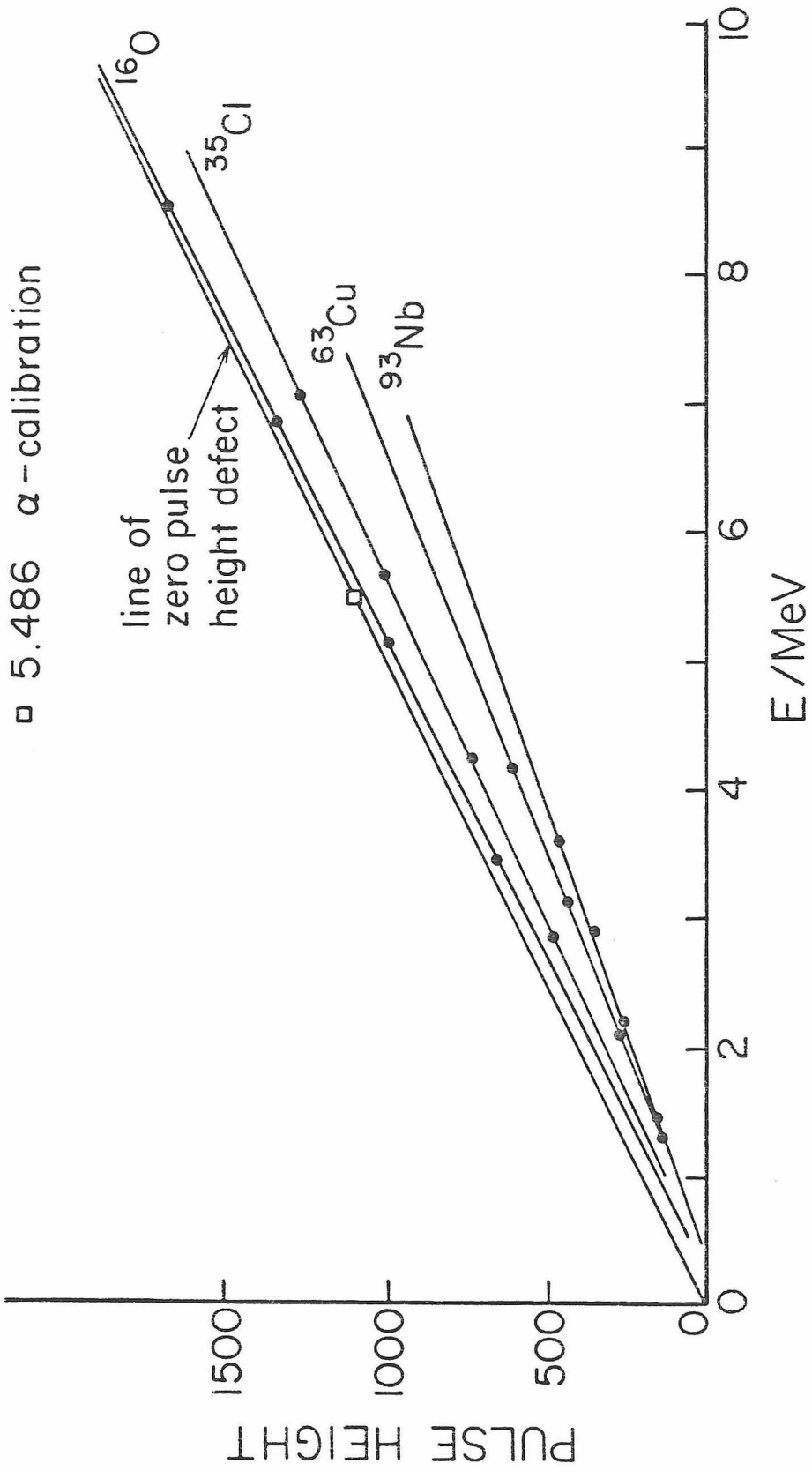
Figure 21

Figure 21 is a plot of pulse height vs. mass for 2 MeV particles incident on the thin silicon detector. The detector was operated at a bias of +33 V and a depletion depth of 20 μm.
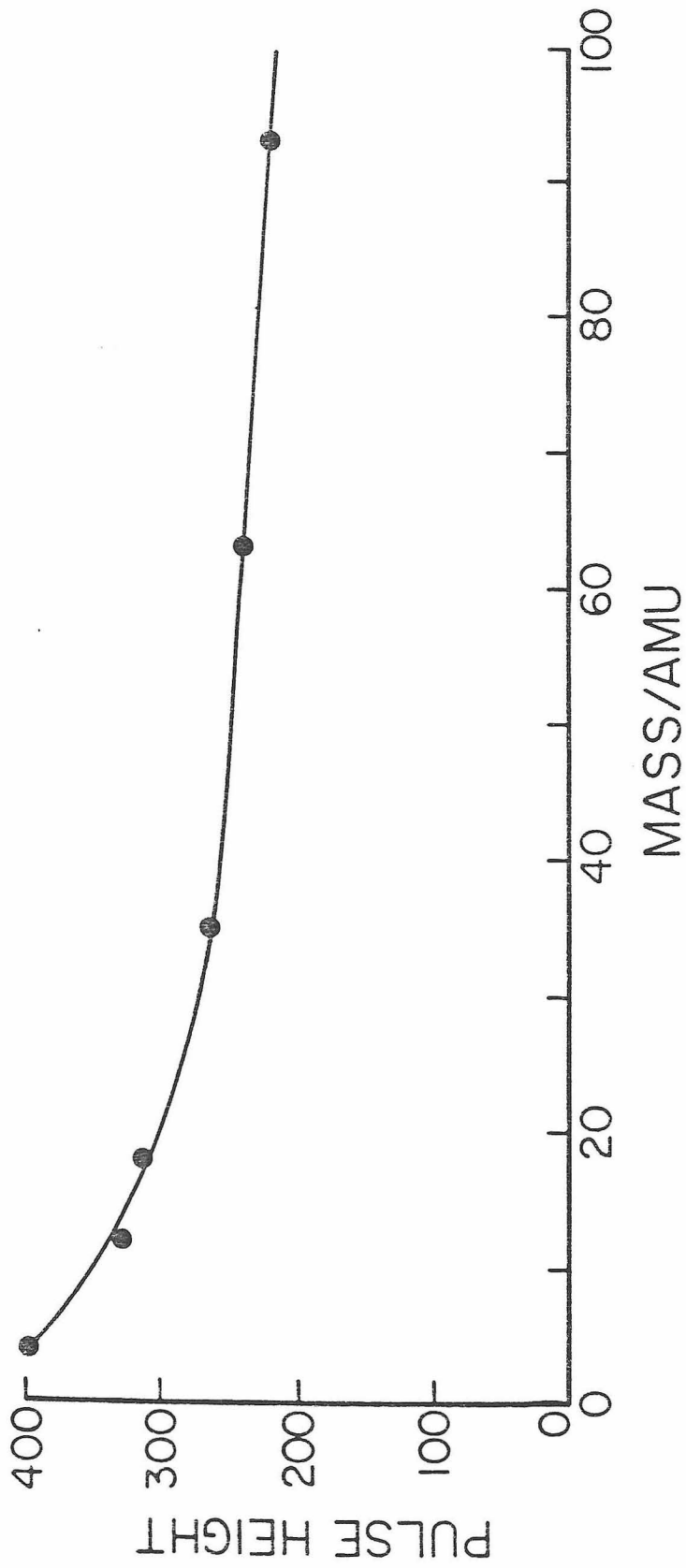
Figure 22

Figure 22 shows pulse height defect data for the gas ΔE detector. These data were obtained by Rutherford scattering through 90° off a 10 μgcm^{-2} gold foil. The data are not corrected for energy lost in the 20 μgcm^{-2} formvar window.
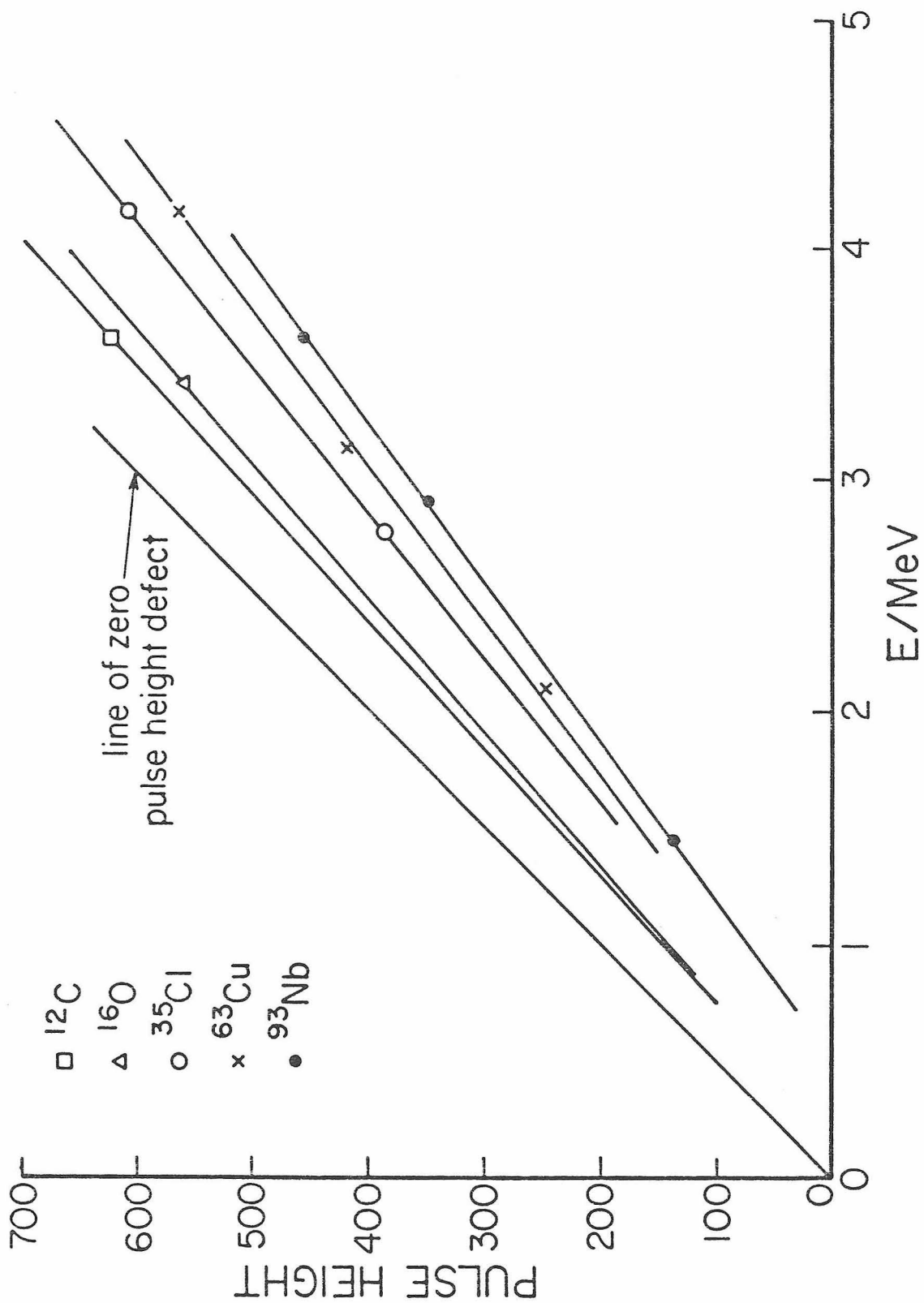
Figure 23

Figure 23 is a plot of pulse height vs. mass for 2 MeV particles incident on the gas ΔE detector.